DFT-Assisted Low-Dimensional Carbon-based Electrocatalysts Design and Mechanism Study: A Review

Yun Han[1,2], *Hongzhe Xu*[1,2], *Qin Li*[1,2], *Aijun Du*[3*], *Xuecheng Yan*[*1]

[1] Queensland Micro- and Nanotechnology Centre, Griffith University, Nathan Campus, QLD 4111, Australia.

[2] School of Engineering and Built Environment, Griffith University, Nathan Campus, QLD 4111, Australia.

[3] School of Chemistry and Physics and Centre for Materials Science, Queensland University of Technology, Gardens Point Campus, Brisbane 4001, Australia.

Corresponding author E-mail: aijun.du@qut.edu.au (A. Du), x.yan@griffith.edu.au (X. Yan)

 doi:10.20944/preprints202211.0444.v1

Abstract

Low-dimensional carbon-based (LDC) materials have attracted extensive research attentions in electrocatalysis because of their unique advantages such as structural diversity, low cost, and chemical tolerance. They have been widely used in a broad range of electrochemical reactions to relief environmental pollution and energy crisis. Typical examples include hydrogen evolution reaction (HER), oxygen evolution reaction (OER), oxygen reduction reaction (ORR), carbon dioxide reduction reaction (CO_2RR), and nitrogen reduction reaction (NRR). Traditional "trial and error" strategies seriously slowed down the rational design of electrocatalysts for these important applications. Recent studies show that the combination of density functional theory (DFT) calculations and experimental research is capable of accurately predicting the structures of electrocatalysts, thus could reveal the catalytic mechanisms. Herein, current well-recognized collaboration methods of theory and practice are reviewed. The history of modern DFT, commonly used calculation methods, and basic functionals are briefly summarized. Special attention is paid to descriptors that are widely accepted as a bridge links the structure and activity, and the breakthroughs for high-volume accurate prediction of electrocatalysts. Importantly, correlating multiple descriptors are used to systematically describe the complicated interfacial electrocatalytic processes of LDC catalysts. In addition, machine learning and high-throughput simulations are crucial in assisting the discovery of new multiple descriptors and reaction mechanisms. This review will guide the further development of LDC electrocatalysts for extended applications from the aspect of DFT computations.

Keywords: Density functional theory, Descriptor, Carbon-based materials, Electrocatalysis, Low dimension.

 doi:10.20944/preprints202211.0444.v1

1. Introduction

Environmental pollution and energy crisis are the two main critical issues of modern society caused by the excessive use of fossil fuels. Acid rain, haze and greenhouse effect have disastrously affected the normal life of human beings.[1-3] On the one hand, great efforts have been devoted to the investigation and utilization of renewable clean energy and the efficient conversion between electrical and chemical energy, i.e., electrocatalytic hydrolysis and fuel cells.[4, 5] Greenhouse gases recycling, on the other hand, is also regarded as one of the most promising techniques to reducing air pollution, for example, the reduction of CO_2. Therefore, effective electrochemical reactions, such as hydrogen evolution reaction (HER) and oxygen evolution reaction (OER) for water splitting, oxygen reduction reaction (ORR) for fuel cell and carbon-dioxide reduction reaction (CO_2RR) are highly expected to solve the above issues (Figure 1).[6, 7] However, the performance of these electrochemical reactions is severely hampered by their sluggish kinetics, which can be significantly improved with the introduction of efficient electrode catalysts.[8, 9]

Noble metal-based materials such as platinum (Pt) and ruthenium (Ru) are widely used as the benchmark catalysts. However, the scarcity and high cost impede their industrial mass production. Therefore, non-noble metal even metal-free electrocatalysts have been intensively studied and remarkable progress has been reached.[10-13] Up to now, low-dimensional carbon materials, such as 2D graphene nanosheets (G), 1D carbon nanotubes (CNT) and 0D fullerenes have been widely used for fabricating a series of non-noble metal and even metal-free catalysts for energy conversion. This is because of their unique properties such as tunable molecular structures, spatial confinement and surface effect, abundance and excellent oxidation and corrosion resistance. Various defects and heteroatoms are embedded into carbon substrates, such as transition metals, nitrogen, boron, *etc.*, which can greatly improve their catalytic efficiency.[14-24]

Preprints (www.preprints.org) | NOT PEER-REVIEWED | Posted: 23 November 2022 doi:10.20944/preprints202211.0444.v1

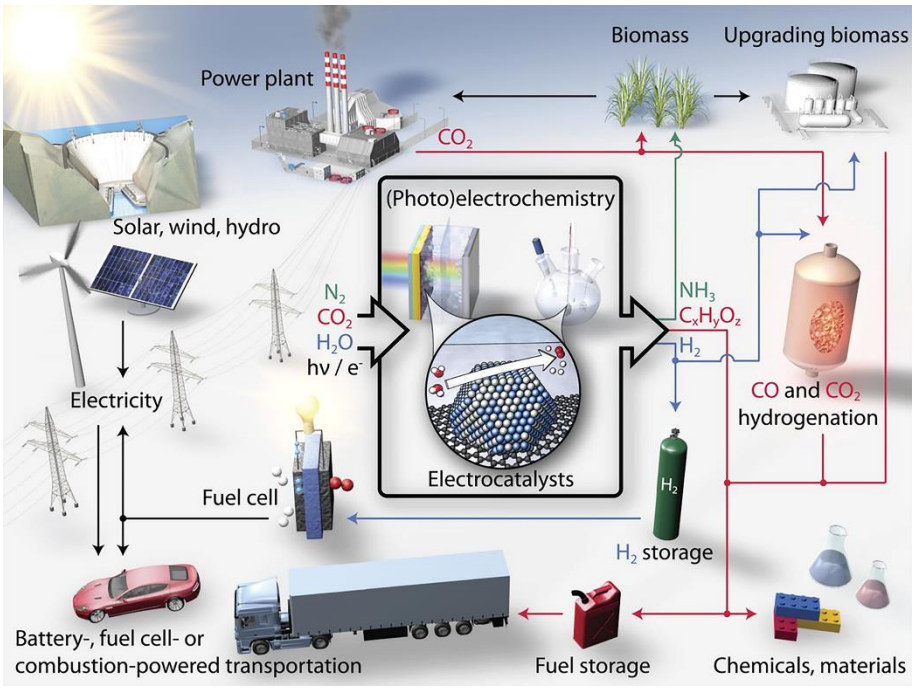

Figure 1. Schematic of a sustainable energy landscape based on electrocatalysis. Reproduced with permission.[6] Copyright 2017, American Association for the Advancement of Science.

It is difficult to reveal the catalytic mechanism and actual active sites of electrocatalysts only *via* experimental study. For instance, previous studies show that pyridinic nitrogen is responsible for the ORR in N-doped carbon-based metal-free catalysts,[25, 26] while other studies suggest that the active sites are graphitic nitrogen.[27, 28] Therefore, the current quest is to develop appropriate methodologies to provide a comprehensive understanding of the catalyst structures at electronic levels, which will promote the comprehension of the reaction mechanisms and guide future experimental study.[29] Nowadays, based on the first principles, the modern density functional theory (DFT) calculation has become an irreplaceable modeling toolkit for scientists in a variety of research areas. Two main strategies of DFT calculation assisted design of electrocatalysts have been established by theoretical and experimental chemists. The first one is dominated by theorical calculations, dedicated to achieving a rational design of high-performance catalysts. It is crucial to identify the most important parameters to reveal the relationships between structures and performance, which is the so-called descriptors and can considerably boost the traditional trial and error approach. Machine-learning and high-throughput calculations also have been developed to efficiently screen active sites and descriptors for the targeted catalysts. The second one is dominated by experimental testing and

Preprints (www.preprints.org) | NOT PEER-REVIEWED | Posted: 23 November 2022 doi:10.20944/preprints202211.0444.v1

characterizations, assisted by calculating the change during the catalysis process such as step-energy, molecular and electronic structure, and electron transition that can reveal the reaction mechanism accurately. In this review, we will mainly summarize the history and concepts of modern DFT, the heterogeneous electrocatalytic surface-related descriptors, the combination of experiment and calculation, and recent achievements of low-dimensional carbon-based electrocatalysts for energy storage and conversation applications.

2. Overview of DFT

Quantum chemistry is mainly based on quantum mechanics principles, and the main goal of all first principle calculations is to obtain the electronic wave function ψ that characterizes the state of the system, for which the Schrödinger equation must be solved. Theoretical computing has received increasing attention from the chemistry community as computer technology has progressed. However, the traditional Wave Function Theory (WFT) method has two fatal shortcomings. First, the wave function ψ of a system with N electrons will contain 3N coordinate variables. Therefore, a 3N-dimensional wave function image, which is difficult to describe visually, will be a stumbling block in solving the Schrödinger equation. Second, the Schrödinger equation for a multi-electron system is too computationally intensive to be calculated accurately. Modern DFT has become a viable option to solve these drawbacks.

2.1 History of Modern DFT

The homogeneous electron-gas model, commonly known as the Thomas-Fermi model, was proposed by Thomas and Fermi in 1927, and it has established a firm foundation for DFT. The ground state energy of the electron system is directly represented in terms of electron density instead of wave function, which drastically reduces the system's freedom degree.[30, 31] In 1964, based on the Thomas-Fermi model, Hohenberg and Kohn proposed an inhomogeneous electron-gas model and proved two theorems served as the fundamentals of modern DFT.[32] The first theorem asserted that the nuclear potential energy $V(r)$ of all electrons in a system has n interacting electrons is a unique function of the electronic density $\rho(r)$. This could be presented as Hohenberg-Kohn equation as shown in Eq. 2.1.

Preprints (www.preprints.org) | NOT PEER-REVIEWED | Posted: 23 November 2022 doi:10.20944/preprints202211.0444.v1

$$E_V[\rho] = \rho(r)V(r)dr + F_{HK}[\rho] \quad \text{Eq. 2.1}$$

Here, $F_{HK}[\rho] = T[\rho] + E_{ee}[\rho]$, $T[\rho]$ is the sum of electronic kinetic energy, $E_{ee}[\rho]$ is electron–electron repulsion. The second theory proposed a density minimum principle, stating that the ground state energy of any trial electron density $\rho(r)$ cannot be lower than the true ground system. Then the Euler-Lagrange equation can be obtained as shown in Eq. 2.2.

$$\mu = \frac{\delta E_V[\rho]}{\delta\rho(r)} = V_{cxt}(r) + \frac{\delta F_{HK}[\rho]}{\delta\rho(r)} \quad \text{Eq. 2.2}$$

Therefore, if $F_{HK}[\rho]$ is confirmed, $\rho(r)$ and $E_V[\rho]$ can be solved by Eq. 2.2. However, the exact expression for $F_{HK}[\rho]$ remains unknown until now. In 1965, Kohn and Sham[33] revealed a brand-new approach to approximately derive the $F_{HK}[\rho]$. $F_{HK}[\rho]$ can be divided into three parts and can be presented as:

$$F_{HK}[\rho] = T_s[\rho] + J[\rho] + E_{xc}[\rho] \quad \text{Eq. 2.3}$$

Where, $T_s[\rho]$ and $J[\rho]$ are the kinetic energy and coulombic correlation energy of independent electrons, respectively. $E_{xc}[\rho]$ is a functional with small magnitude called exchange–correlation (XC) energy that can be approximated, and it can be presented as:

$$E_{xc}[\rho] = T[\rho] - T_s[\rho] + V_{ee}[\rho] - J[\rho] \quad \text{Eq. 2.4}$$

By variation, we can get the famous Kohn-Sham equation:

$$\widehat{H}_{KS}\emptyset_i \equiv \left[-\frac{1}{2}\nabla^2 + V(r) + \int \rho\left(r'\right)\Big/\left|r - r'\right| dr' + V_{xc}(r)\right]\emptyset_i(r) = \varepsilon_i\emptyset_i(r) \quad \text{Eq. 2.5}$$

And XC potential can be defined by:

$$V_{xc}(r) = \delta E_{xc}[\rho]/\delta\rho(r) \quad \text{Eq. 2.6}$$

Overall, there is no approximation and the Kohn-Sham equation is accurate. However, the $E_{xc}[\rho]$ component of the Kohn-Sham equation still lacks a rigors expression form, making it impossible to use in practical calculations. Instead, several types of approximate XC generalized functionals must be built to gradually approximate the real system.

Preprints (www.preprints.org) | NOT PEER-REVIEWED | Posted: 23 November 2022 doi:10.20944/preprints202211.0444.v1

2.2 Exchange–Correlation (XC) Functional

Some of the approximations such as local density approximation (LDA), generalized gradient approximation (GGA), meta-GGA, and hybrid functional can be shown as the well-known Jacob's ladder from Hartree world to Chemical accuracy heaven (Figure 2).[34-36]

Figure 2. Illustration of Jacob's Ladder of DFT. Reproduced with permission.[36] Copyright 2020, John Wiley and Sons.

The approximation for LDA is that the charge density changes slowly with position and behaves similar to local heterogeneous electron cloud, so the XC energy can be presented as:

$$E_{XC}^{LDA}[n] = \int drn(r)\varepsilon_{XC}(n) \qquad \text{Eq. 2.7}$$

However, the LDA method is rough in calculating the actual system and will overestimate the binding energy of the electron density because of their localized character.

To improve the accuracy of the LDA method, GGA method describes electron density with the assistance of density gradient, and can be presented as:

$$E_{XC}^{GGA} \propto \int drf(n, \nabla n) \qquad \text{Eq. 2.8}$$

Preprints (www.preprints.org) | NOT PEER-REVIEWED | Posted: 23 November 2022 doi:10.20944/preprints202211.0444.v1

BLYP,[37, 38] PW91,[39, 40] and PBE[41] are the commonly used approximated density functionals of GGA method.

Based on the GGA method, meta-GGA, such as TPSS, TPSSh, and M06-L,[42-44] introduced kinetic energy density variables, but with better accuracy accompanied by a significant increase in computational cost.

By partially combining accurate XC functional in the DFT, the hybrid functional could improve the calculation accuracy. The most popular one is the B3LYP functional,[45] which can be described as:

$$E_{XC}^{B3LYP} = A \cdot E_X^{LDA} + (1-A)E_X^{HF} + B \cdot \Delta E_X^{Beck} + C \cdot E_C^{LYP} + (1-C)E_C^{VWN} \quad \text{Eq. 2.9}$$

Calculations involving periodic systems frequently employ the HSE functional,[46] which is represented by the following equation:

$$E_{XC}^{HSE} = A \cdot E_X^{HF,SR} + (1-A)E_X^{PBE,SR} + E_X^{PBE,LR} + E_C^{PBE} \quad \text{Eq. 2.10}$$

2.3 Periodic System

To deal with periodic systems, supercell models (primitive cells in three dimensions (X, Y, and Z) with periodic repetition) are frequently used. Vacuum space greater than 10 Å is added in the Z-direction to eliminate the interaction. In condensed matter physics, Bloch's theorem states that solutions to the Schrödinger equation in a periodic potential take the form of a plane wave modulated by a periodic function, and can be written as:

$$\Psi(r) = u_k(r)e^{ikr} \quad \text{Eq. 2.11}$$

Where r is the position, Ψ is the wave function, k is the wave vector. Based on the Bloch theorem, electronic band structure is involved to investigate the surface science, and electronic states at numerous k points should be calculated. In practical calculations, however, a finite number of k points are used, the higher the density of the k points, the lower the inaccuracy will be. In general, the numbers of k points for metal systems are higher than that of the oxide systems.

For periodic systems, electron wave function can be expanded with numerous plane-wave functions. However, only plane-wave basis sets with kinetic energy lower than the cut-off

Preprints (www.preprints.org) | NOT PEER-REVIEWED | Posted: 23 November 2022 doi:10.20944/preprints202211.0444.v1

energy are considered in practical calculations, which would result in a systematic error.[47, 48] Therefore, pseudopotential that can replace the true atomic potential of the nucleus and inner electrons, is introduced to reduce the systematic error. Currently, the most widely used plane wave methods are ultra-soft pseudopotentials (US-PP) plane wave method and projector augmented wave (PAW) method.[49]

2.4 DFT+U Scheme

DFT calculations cannot adequately describe systems with physical properties that are controlled by many-body electronic interactions (correlated systems), because it is typically challenging to model the dependence of the XC functional on electronic charge density. The over-delocalize valence electrons and over-stabilize metallic ground states are considered to be the main problems of DFT to describe correlated systems. Therefore, the DFT+U approach has been developed to enhance the description of the ground state of correlated systems.[50] The key advantage of the DFT+U method is that it is within the realm of DFT, which makes it easy to implement in the existing DFT codes and its computational cost is only slightly higher than that of normal DFT computations. The local and semi-local density functionals that allow LDA+U and GGA+U computational operations can be enhanced with this 'U' correction. The primary function of the 'U' correction is to add an additional Hubbard-like term to the strong on-site Coulomb interaction of localized electrons. The on-site Coulomb term U and the site exchange term J are the two parameters that represent the strength of the on-site interactions for the purpose of practical DFT+U implementation in computational chemistry. Parameters 'U and J' are typically derived semi-empirically, although *ab initio* computations can yield them.[51]

$$E(DFT+U) = E(DFT) + {}^{U_{eff}}/_{2} \sum_{\sigma} Tr[\rho^{\sigma} - \rho^{\sigma}\rho^{\sigma}] \qquad \text{Eq. 2.12}$$

It has become a standard to use the parameter: $U_{eff} = U - J$ in place of the interaction parameter U in the simplified LDA+U form. U_{eff} is frequently preferred, because the 'J' parameter has been shown to be essential for describing the electronic structure of specific classes of materials, typically those subject to high spin-orbit coupling.

Preprints (www.preprints.org) | NOT PEER-REVIEWED | Posted: 23 November 2022 doi:10.20944/preprints202211.0444.v1

2.5 Molecular Dynamics Simulation

Molecular dynamics (MD) simulation, which is based on Newton's laws of motion, can simulate the trajectory of each atom in a system at a certain temperature, thus the system's dynamic properties can be calculated. However, the standard DFT can only be used to calculate a system's static properties at 0 K. Briefly, for a given configuration and initial velocity of each atom, the MD simulation can be divided into three steps. First of all, the forces acting on each atom in the system are calculated to determine the system's acceleration. Secondly, the configuration of the system after Δt time can be obtained according to the Newton's three laws. Thirdly, the calculation of the forces in the first step is continued based on this configuration, and the results of the system evolving with time can finally obtain by repeated recurrence.

MD simulation can be further classified into two types: Classic MD simulation and *ab initio* MD (AIMD) simulation, depending on how the forces are calculated in the first step. Classic MD simulation builds the potential energy function from the empirical force field and calculates the force at each step using the gradient of the potential energy function. AIMD simulation, on the other hand, can be used to accurately calculate the force at each step by the *ab initio* quantum chemical method.[52-54]

2.6 Transition State Theory

The transition state (TS), also known as the saddle point, is the highest energy point on the potential energy surface (PES) where the reactants (initial state, IS) generate products (final state, FS) along the minimum energy path. Within the transition state theory (TST), we assume that IS and TS are in the quasi-equilibrium, and the main task is to find out the free energy barrier for the transition, which is the energy difference between IS and FS. Based on TST, transition rate can also be calculated. The Dimer method[55] and the climbing image nudged elastic band (CINEB) approach[56] are the two most popular calculating techniques.

The dimer method can be used to find out the saddle points by two images of the system, which is the so-called 'dimer'. Driving by the saddle point search algorithm, dimer is moved uphill on the potential energy surface, away from the vicinity of the potential energy minimum of the IS and toward a saddle point. The dimer is rotated along the way to identify the potential energy mode with the lowest curvature at the dimer's location. Since the Dimer technique only uses the

Preprints (www.preprints.org) | NOT PEER-REVIEWED | Posted: 23 November 2022 doi:10.20944/preprints202211.0444.v1

first derivatives of the energy, the major benefit is not requiring the time-consuming computation of the minimal eigenvalue of the Hessian matrix. The Dimer technique also has the advantage of having less stringent initial configuration requirements.

The nudged elastic band (NEB) method is an efficient method for identifying the minimum energy path (MEP) between a given initial and the final state of a transition, which has also been widely used to estimate transition rates. A set of images between the IS and FS of the system are created, often on the order of 4-20. Then the adjacent images are contacted by a collection of spring interactions, which can form an elastic band and ensure the continuity of the path. The band is brought to the MEP by an optimization process that minimizes the force acting on the images. The drawback of the NEB method is that it requires the intermediates be evenly spaced throughout the optimization process, the predicted TS may be slightly deviated from the actual TS. The CINEB method was developed to address this issue, and the force on the highest image is the full force resulting from the potential with the component along the elastic band inverted, showing that it will not be impacted by spring forces. As a result, the intermediate will gradually move to the direction of higher energy and reaches the actual TS.

3. Theoretical Guidance in Catalyst Design and Mechanism Study

Nowadays, a series of well-known carbon-based electrocatalysts have been fabricated through the combinations of various modification methods and substrate materials, such as heteroatom doped graphene, defective graphene, Mxene, heteroatom doped carbon nanotubes/ribbons and modified carbon dots.[57-65] However, the design of state-of-the-art electrocatalysts still relies on inefficient trial-and-error approaches, and the catalytic mechanism is still controversial and difficult to reveal only through experimental research. DFT calculations are thus utilized to address two issues: 1) predicting catalytic performance and guiding the synthesis of electrocatalysts. 2) investigating and corroborating the mechanism of electrocatalysis in conjunction with experimental study.

3.1 Application of Theoretical Guidance in Designing Electrocatalysts: Descriptors

To predict the performance of electrocatalysts, computational scientists mainly focus on the most important microscopic properties of the catalysts that determine the macroscopic catalytic performance. Since early 20th century, catalysts with high activity, according to the traditional

Preprints (www.preprints.org) | NOT PEER-REVIEWED | Posted: 23 November 2022 doi:10.20944/preprints202211.0444.v1

Sabatier principle, should bind atoms and molecules with an ideal bond strength: not too weak to activate the reactants, and not too strong to desorb the products. Therefore, a volcano shape relationship between bond strength and catalytic activity has been proposed to represent the predictivity of many descriptors.[66] Due to the lack of quantitativeness and inability to undergo experimental validation, this principle is not very predictive. The "bond strength" between the relevant intermediates and the catalysts has been described during the past decades by the extraction of electronic and structural properties such as the descriptors.

3.1.1 *d*-Band Center Theory

The well-known *d*-band center theory proposed by Nørskov *et al.* has laid the foundation for a series of descriptors.[67-69] It explains the interactions between atoms or molecules and the surface based on adsorbate orbitals and *d*-orbitals of atoms on the surface. The energy of the *d* states (the center of the *d* states) relative to the Fermi level is a good first indicator of the bond strength. The higher the *d* states are in energy relative to the Fermi level, the higher in energy the antibonding states and the stronger the bond will be (Figure 3).

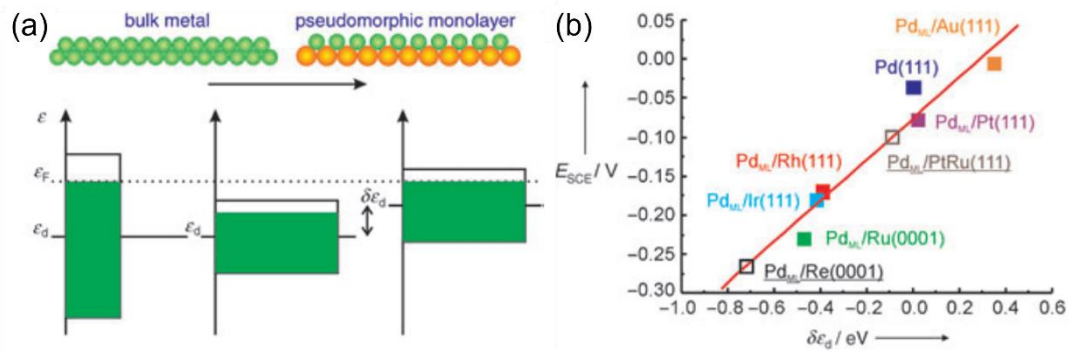

Figure 3. Illustration of the use of the *d*-band model. (a) The main origin of a shift in the *d*-band center ε_d is a change in the interatomic distances within an overlayer. (b) Electrochemically measured changes in the hydrogen adsorption energy (E_{SCE}) for Pd overlayers on a number of metals are shown to scale well with the calculated shift of the *d*-band center ($\delta\varepsilon_d$). Reproduced with permission.[70] Copyright 2005, John Wiley and Sons.

The *d*-band center theory can also be applied on low-dimensional carbon-based

Preprints (www.preprints.org) | NOT PEER-REVIEWED | Posted: 23 November 2022 doi:10.20944/preprints202211.0444.v1

electrocatalysts.[71-75] For instance, Deng *et al.* designed a series of N-doped graphene-supported transition metal atom-pair catalysts (TM APCs) models for efficient NRR.[76] Twenty kinds of transition metal atoms were systematically studied and were proven by COHP and orbital interaction analysis, the *d*-band center can be used as a descriptor to describe the NRR performance of the TM APCs. For defective graphene-supported Fe and Al nanoparticles, Lim and co-workers found that the *d*-band center of the Fe and Al nanoparticles shift closer to the Fermi level, indicating a potential increase in the catalytic reactivity associated with the graphene surface. Zhou *et al.* systematically explored the HER activity of transition metals, transition metal oxides and carbides substrates covered by nitrogen-doped graphitic sheets and found that the HER activity is correlated to the C p_z-band center, which is similar to the *d*-band center theory and determined in turn by the degree of electronic coupling between the graphitic sheet and the metal substrate, enabling the rational design of high-performance hybrid graphitic carbon/transition metal electrocatalysts.[77]

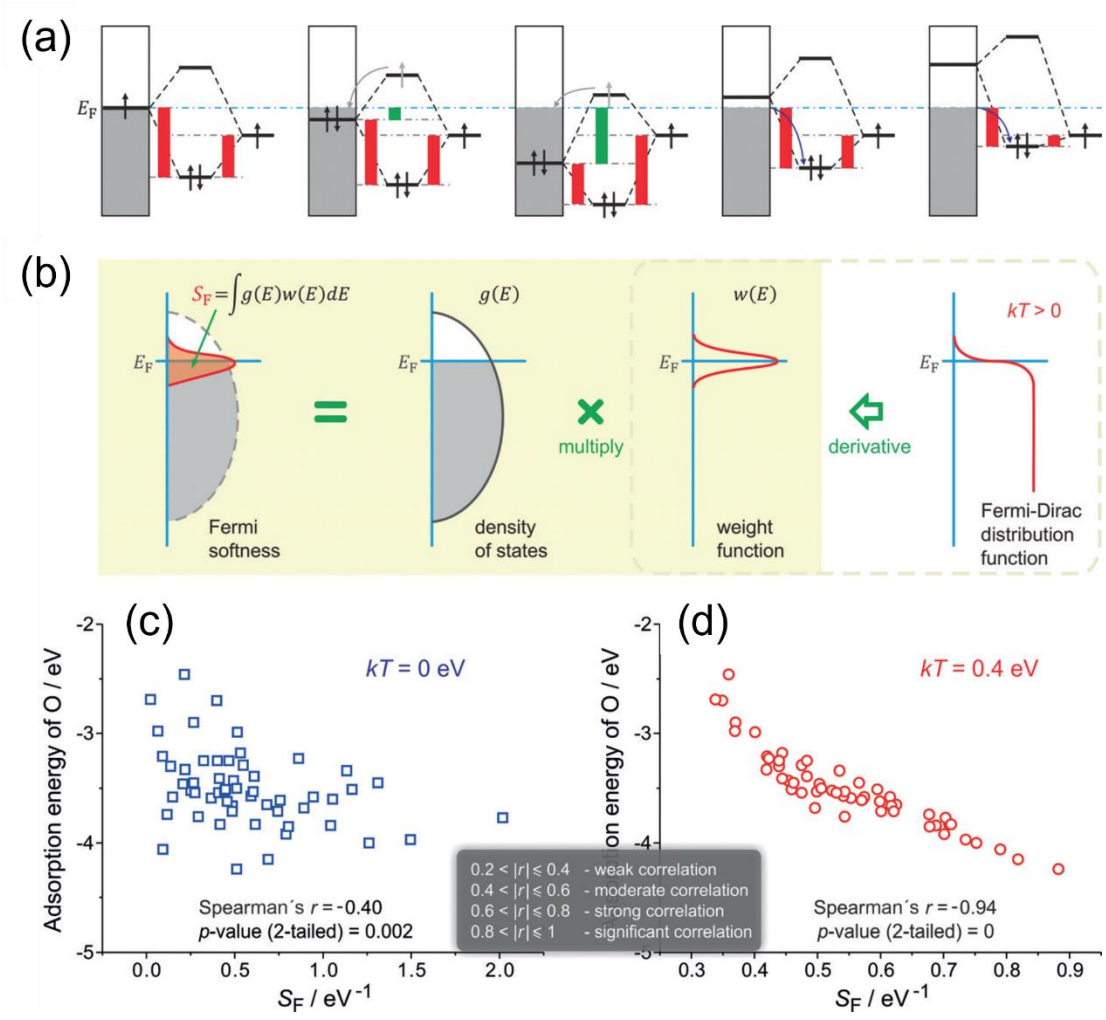

Preprints (www.preprints.org) | NOT PEER-REVIEWED | Posted: 23 November 2022 doi:10.20944/preprints202211.0444.v1

Figure 4. Definition of Fermi softness (S_F) and its correlation with surface reactivity. Reproduced with permission.[78] Copyright 2016, John Wiley and Sons.

3.1.2 Fermi Softness

When oxygen atoms adsorbed on Pt_3Y (111) surface, even though the surface *d*-band center of Y is higher than that of Pt, the binding strength of Pt-O is stronger than Y-O, defying the *d*-band center theory. However, it can be reasonably explained by the "Fermi softness" (S_F), which was developed by Huang and co-workers for describing the electronic structures of a solid surface.[78] All the band's occupied and unoccupied states contribute to the bonding, but those closer to the Fermi level (E_F) are more significant (Figure 4A). To determine a weighted summation of the density of states of a solid surface ($\int g(E)w(E)dE$), a reactivity weight function *w(E)* with a Fermi level peak is created (Figure 4B). The resultant property is the finite-temperature chemical softness, known as S_F, which is an accurate descriptor of the surface reactivity. This property is obtained when such a weight function is defined as the derivative of the Fermi-Dirac distribution function at a certain non-zero temperature. For example, the S_F is identical to the density of states at Fermi level ($g(E_F)$) without spreading (i.e., kT = 0 eV), which does not closely resemble the surface reactivity (Figure 4C). Then, the S_F displays a substantial association with the surface reactivity when the nominal electronic temperature is changed to 0.4 eV (Figure 4D).

Fermi softness can also be an efficient descriptor to predict the catalytic performance of carbon-based catalysts.[79-83] Gao and co-workers designed a series of catalysts named Fe/GS, which are composed of Fe atom serves as the active site and different graphene such as single and double vacancy graphene serves as the substrate.[81] They further demonstrated that Fermi softness of Fe/GS and the O_2 adsorption energy exhibit a strong positive linear correlation (R^2 = 0.81) at kT = 1.15 eV. Fermi softness is also used to describe the adsorption activity of Mn-modified graphene catalyst by Wu's group.[84] They discovered a substantial negative correlation (R^2 = 0.93) between Fermi softness and adsorption energy at kT = 2.8 eV. The Fermi softness is increased with the increase of the adsorption energy.

Preprints (www.preprints.org) | NOT PEER-REVIEWED | Posted: 23 November 2022 doi:10.20944/preprints202211.0444.v1

3.1.3 Linear Scaling Relationships

In multi-step catalytic processes, the adsorption and desorption of the intermediates occur during the concerted proton–electron transfer steps, and the adsorption energies of the intermediates follow a linear scaling relationship.[85, 86] For example, the relationship between the adsorption energies of the intermediates of OER and ORR, such as *O, *OH, and *OOH, can be presented by:

$$\Delta G_2^{(i)} = A_{1,2}^{(i)} \cdot \Delta G_1^{(i)} + B_{1,2}^{(i)} \quad \text{Eq. 3.1}$$

Where $\Delta G_1^{(i)}$ and $\Delta G_2^{(i)}$ represent the chemisorption energies of oxygen intermediates.[87, 88] Fundamentally, the quantity of valence electrons of the atoms attached to the surface has a significant impact on the slope of Eq. 3.1 on closed-packed and low-index surfaces. Since the oxygen atom in OH* only requires one electron to comply with the octet rule, whereas O* requires two, the slope between the adsorption energies of *OH and *O is roughly 1/2. Scaling relationships offer a chance for using a few descriptors to fully present the numerous factors affecting a full catalytic reaction. Combined with the Sabatier principle, volcano curves can be derived from this linear relationship to reveal the connection between structures and performance. In many cases, ΔG_{OH} and $\Delta G_O - \Delta G_{OH}$ are considered as the descriptors for ORR and OER, respectively.[89-91] According to the statistical findings, the free energy difference for monodentate adsorbates can be concluded as $\Delta G_{OOH} = \Delta G_{OH} + 3.2 \pm (0.2)$ eV.[85]

Preprints (www.preprints.org) | NOT PEER-REVIEWED | Posted: 23 November 2022 doi:10.20944/preprints202211.0444.v1

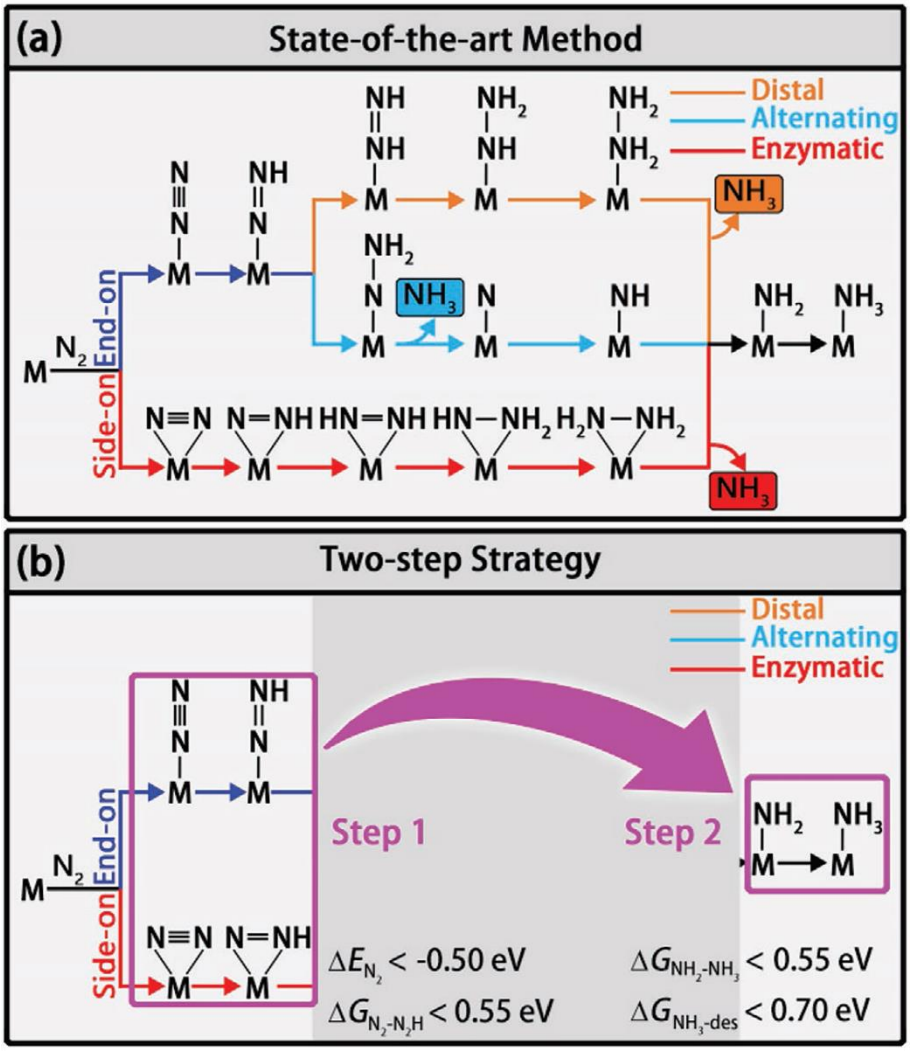

Figure 5. (a) Schematic depiction of different mechanisms for N_2 reduction. (b) Flowchart of the two-step screening procedure for NRR catalysts. Reproduced with permission.[92] Copyright 2018, John Wiley and Sons.

3.1.4 Multiple Descriptors

The excellent descriptors include e_g-filling,[93, 94] average O-*2p*-state energy ($\bar{\varepsilon}_{2p}$),[95, 96] surface distortion,[97] and generalized coordination numbers ($\overline{CN}$).[98, 99] Normally, single descriptor cannot completely predict the performance and synergistic effect of complicated mixed-phase catalysts. Some interface parameters that can demonstrate or influence electron distribution reconfiguration, for instance, adsorption energy,[100-102] charge transfer,[103, 104] surface properties (defects/microstructure/facet),[105, 106] and bond length[107-109] may serve as the descriptors to

Preprints (www.preprints.org) | NOT PEER-REVIEWED | Posted: 23 November 2022 doi:10.20944/preprints202211.0444.v1

predict the best catalysts. Furthermore, a variety of descriptors have been used for the description of the reactions with the assistance of machine learning and high-throughput calculations.

The complex NRR can occur through different mechanisms, including distal, alternating, and enzymatic (Figure 5a). To identify the viable routes and theoretical onset potentials by the classical approach, all chemical intermediates will be systematically investigated, which will be inefficient for large-scale catalyst screening. Ling *et al.* focused on two "stable to instable" transitions in the NRR process (Eq. 3.2 and 3.3) and set up a two-step method (Figure 5b) to efficiently and accurately screen the nitride-doped-graphene supported single atom catalysts (N-G-supported SACs).[92]

$$* N_2 + H^+ + e^- = * N_2H \qquad \text{Eq. 3.2}$$

$$* NH_2 + H^+ + e^- = * NH_3 \qquad \text{Eq. 3.3}$$

In the first step, the systems with low activity are disregarded by using the descriptors ΔE_{N_2} (adsorption energy of N_2) and $\Delta G_{N_2-N_2H}$ (free energy change of Eq. 3.2). In the second step, among the systems that met the requirements of the step one, high performance catalysts are sought after using the descriptors ΔG_{NH_3-des} (free energy for NH_3 desorption) and $\Delta G_{NH_2-NH_3}$ (free energy change of Eq. 3.3). Out of 540 N-G-supported SACs systems, ten interesting candidates with high NRR catalytic activity were selected using the two-step high-throughput screen approach. For example, W_1C_3 demonstrates the best performance with an incredibly low onset potential of 0.25 V. Zhou and co-workers also used multiple descriptors to predict the NRR catalytic performance of transition metal atoms filled boron nitride nanotubes (BNNTs).[57] The diameter of BNNTs, work function and electron transfer from metal to BNNTs, which have negative correlations with the adsorption energy of N_2, can serves as efficient descriptors to select highly active catalysts.

3.2 Application of Theoretical Calculations in Revealing the Reaction Mechanism

With the development of modern characterization techniques, an increasing number of *in situ* characterization tools are used to observe the catalytic reaction processes, aiming to accurately uncover the catalytic mechanism. However, it is still difficult to identify the actual active site

Preprints (www.preprints.org) | NOT PEER-REVIEWED | Posted: 23 November 2022 doi:10.20944/preprints202211.0444.v1

and reaction intermediates of complex catalytic reactions by pure experimental study. For example, through different reaction routes, the products of CO_2RR can be carbon monoxide, formic acid, ethylene, or ethanol. Depending on whether the adsorption sites change or not during the catalytic processes, the actual reaction paths and intermediates, the competition between carbon-carbon coupling reaction and HER are all unknown and difficult to elucidate experimentally.[110] Theoretical calculation is a key method to compensate for experimental shortcomings because it can investigate the electronic-scale change during the catalytic reaction. In the past decades, the use of theoretical simulations in defective electrocatalysis has greatly aided the design of novel catalysts.[111-114]

With the assistance of DFT calculations, Zhang *et al.* systematically investigated the origins of the high-performance atomic Co-Pt embedded into nitrogen doped graphene (A-CoPt-NC).[115] A stable adsorption state of the intermediate in the HER is proved by the electron distribution calculations. The disappearance of charge depletion on the surface of the outer layer can improve the adsorption of protons to the catalyst. Li and co-workers synthesized a new type of high-performance HER electrocatalyst.[116] Carbon quantum dots were used to support ruthenium nanoparticle (Ru@CQDs), and it shows superior catalytic activity and durability in alkaline conditions than the state-of-the-art commercial Pt/C catalyst. DFT calculations provide compelling evidence to the excellent HER catalytic activity of Ru supported in the N-doped CQDs layer. The calculation results show the synergistic effect of doped N atoms and Ru clusters, both are beneficial to reduce the dissociation energy of H_2O. The electron transfer from Ru and H_2O to C atoms, which is proved by the difference charge density analysis, can polarize Ru clusters, thus contributed to the dissociation of H_2O. Meanwhile, the dissociated H atoms are held together by Ru and H interactions to form the H_2 molecule (Figure 6).

Preprints (www.preprints.org) | NOT PEER-REVIEWED | Posted: 23 November 2022 doi:10.20944/preprints202211.0444.v1

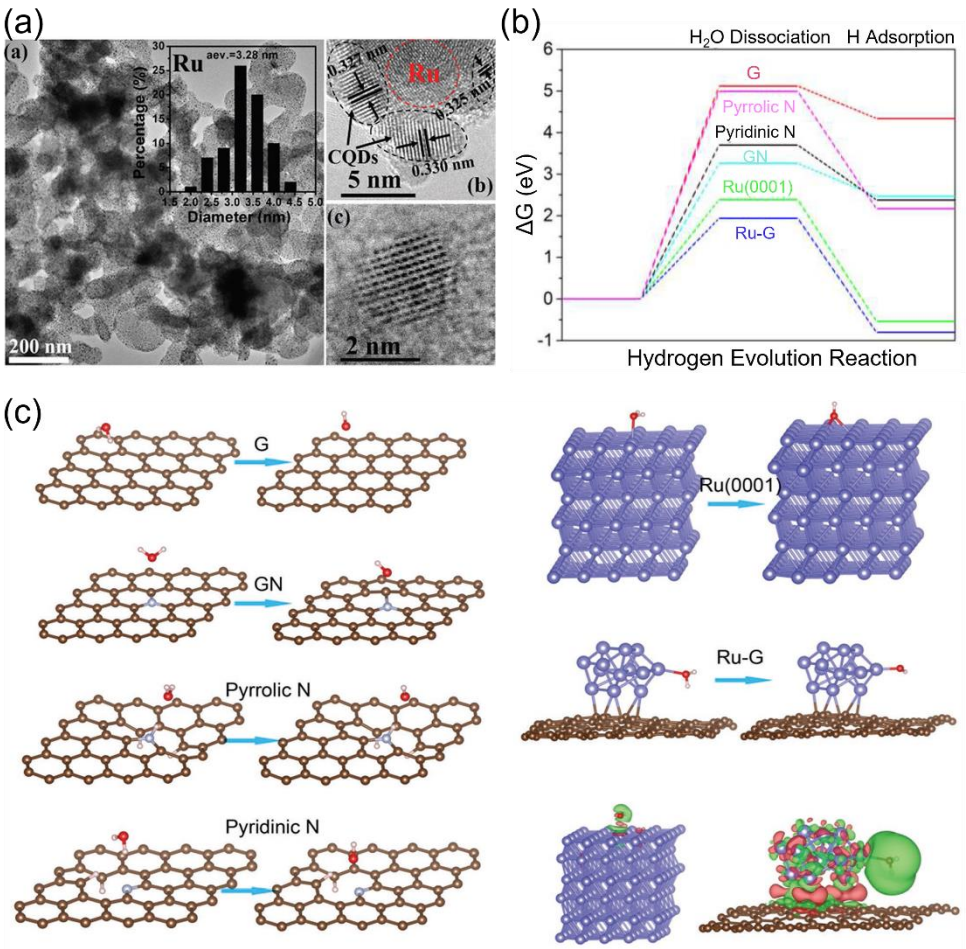

Figure 6. (a) TEM and HRTEM images of Ru@CQDs. (b) Calculated HER relative energy diagram. (c) Adsorption and dissociation of the H_2O molecule on difference surfaces. Reproduced with permission.[116] Copyright 2018, John Wiley and Sons.

As can be seen from the above discussions, theoretical calculation is an indispensable method to investigate the relationship between structures and performance. A plausible reaction model will be built to thoroughly study the basic reaction path of the reaction and identify the crucial steps that determine the reaction rate, and then to optimize the chemical reaction conditions. It is obvious that theoretical calculations are beneficial in identifying the basic process and reaction paths of the electrocatalysis at the atomic level. Furthermore, the design of catalysts and the controlled synthesis of the desired structures can be aided by the DFT simulations, which can be utilized as a prediction tool. Theoretical modellings can also be used in catalyst structure optimization, validation of the design outcomes, and support experimental study.

Preprints (www.preprints.org) | NOT PEER-REVIEWED | Posted: 23 November 2022 doi:10.20944/preprints202211.0444.v1

4. Recent Advances in Computational Studies on Low-Dimensional Carbon-based Electrocatalysts

4.1 Hydrogen Evolution Reaction (HER)

Hydrogen is one of the most promising clean energy sources to replace fossil fuels, it also has the highest energy density among existing fuels. Water splitting is a sustainable way of producing hydrogen compared to industrial reduction of natural gas (CH_4). Hydrogen evolution reaction (HER) is the cathodic half-cell reaction of water electrolysis,[7] the large overpotential restricts its practical application and high performance electrocatalysts are needed to boost the HER. Noble metal-based catalysts such as Pt/C and RuO_2 are commonly considered to be the most efficient HER electrocatalysts, however, the scarcity and low durability limit their mass industrial production.[117, 118] To date, many high performance low-dimensional carbon-based non-noble metal even metal-free electrocatalysts have been designed and fabricated to be the alternatives of noble metal materials. In this part, the fundamental concepts and recent development on HER electrocatalysts will be summarized.

HER is a two proton-electron transfer steps (PETS) process, the first step is Volmer reaction, i.e., the adsorption of hydrogen, which can be present by Eq. 4.1a (acidic condition) and 4.1b (alkaline condition).

$$H^+ + e^- + * \rightarrow H^* \qquad \text{Eq. 4.1a}$$

$$H_2O + e^- + * \rightarrow H^* + OH^- \qquad \text{Eq. 4.1b}$$

The second step can be the Heyrovsky reactions or Tafel reaction, Eq. 4.2a (acidic condition) and 4.2b (alkaline condition) show the Heyrovsky reactions, and Eq. 4.3 show the Tafel reaction.

$$H^* + H^+ + e^- \rightarrow H_2 + * \qquad \text{Eq. 4.2a}$$

$$H^* + H_2O + e^- \rightarrow H_2 + OH^- + * \qquad \text{Eq. 4.2b}$$

$$2H^* \rightarrow H_2 + * \qquad \text{Eq. 4.3}$$

In which, * represents the active site on the catalyst surface.

Preprints (www.preprints.org) | NOT PEER-REVIEWED | Posted: 23 November 2022 doi:10.20944/preprints202211.0444.v1

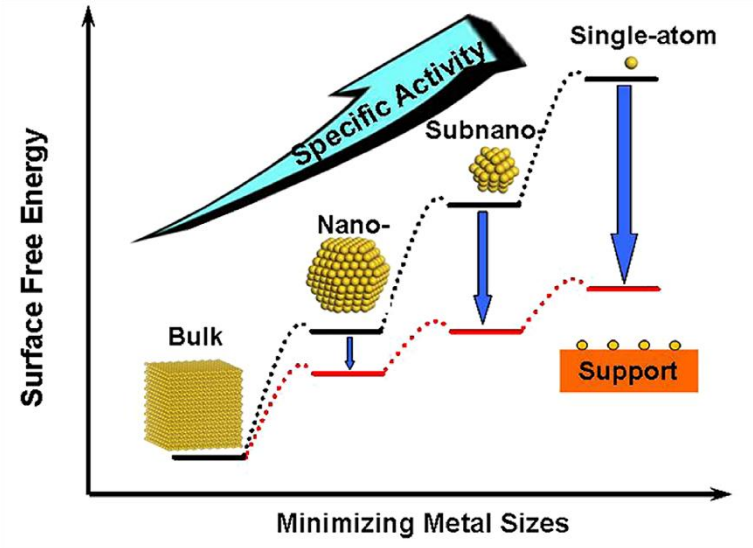

Figure 7. Schematic illustration of the changes of surface free energy and specific activity per metal atom with metal particle size and the support effects on stabilizing single atoms. Reproduced with permission.[119] Copyright 2013, American Chemical Society.

Preprints (www.preprints.org) | NOT PEER-REVIEWED | Posted: 23 November 2022 doi:10.20944/preprints202211.0444.v1

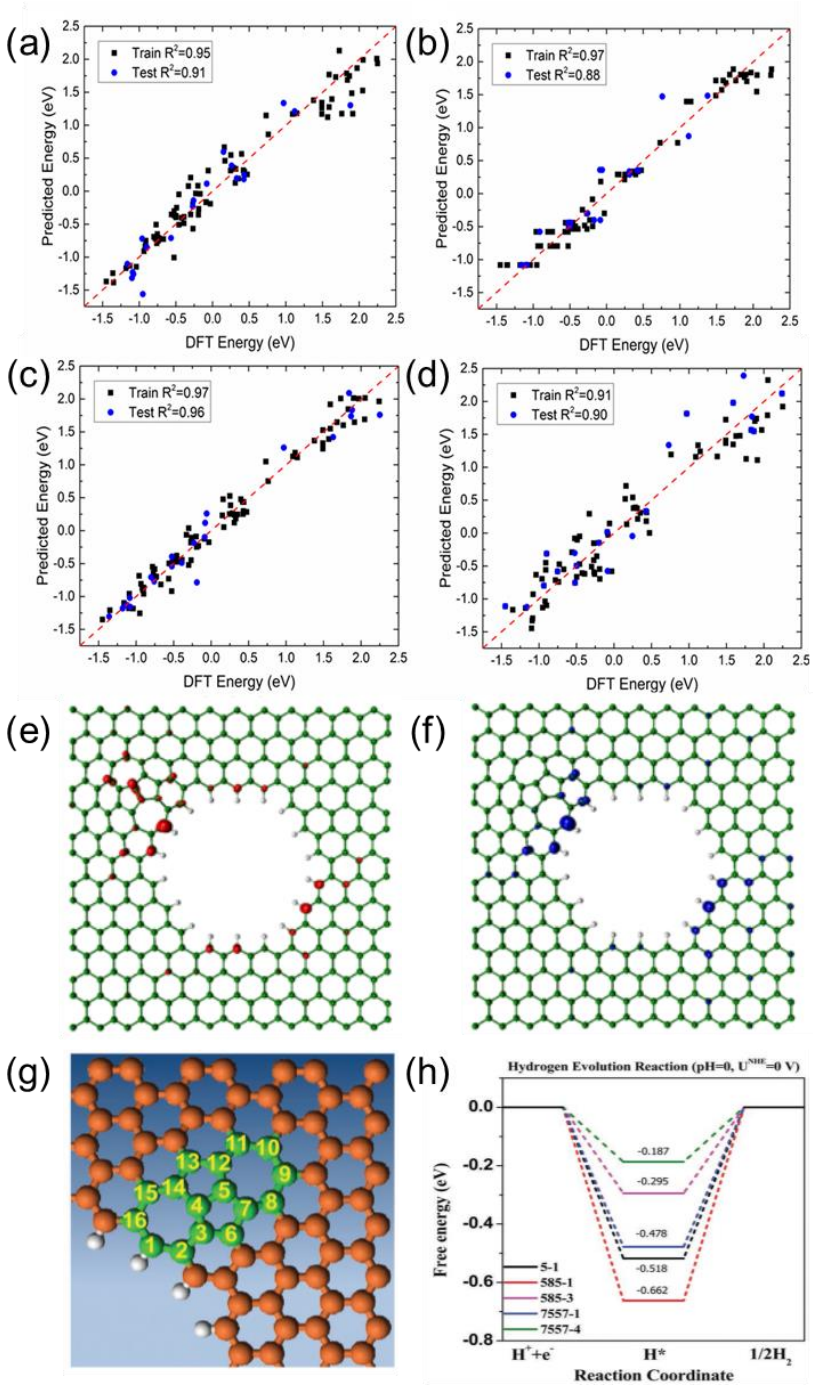

Figure 8. Comparison of DFT calculated versus machine learning predicted ΔG_H using (a) kernel ridge regression, (b) random forest regression, (c) neural network regression, and (d) SISSO regression. Reproduced with permission.[131] Copyright 2020, American Chemical Society. (e) HOMO and (f) LUMO orbitals for 7557 defect. (g) Mechanism study model of 7557defect. (h) Schematic energy profiles for the HER pathway. Reproduced with permission.[16] Copyright 2016, John Wiley and Sons.

Preprints (www.preprints.org) | NOT PEER-REVIEWED | Posted: 23 November 2022 doi:10.20944/preprints202211.0444.v1

For the design of low-cost and efficient electrocatalysts, it is crucial to reduce the amount of precious metals being used, which can be achieved in two ways. Firstly, the specific activity per metal atom usually increases with the downsize of metal particles (Figure 7).[119] Therefore, a new kind of electrocatalyst called single-atom catalyst (SAC), which contains isolated metal atoms singly dispersed on supports, has attracted extensive research attentions. Alternatively, non-noble metal atoms or functional groups can also be anchored on the substrate to tune the electronic structures of noble-metal active sites.[120-124] Ye and co-workers designed a novel Pt SAC, using aniline-stacked graphene as the support (Pt SASs/AG). It shows excellent HER performance with η = 12 mV at 10 mA cm^{-2} and a mass current density of 22400 Ag_{Pt}^{-1} at η = 50 mV, which is 46 times higher than that of the commercial 20 wt% Pt/C.[125] Moreover, the Pt SASs/AG catalyst presents outstanding stablity. With the assisstance of DFT calculations, they found that the interaction between the atomical Pt and the nitrogen of aniline makes the *d*-band center of Pt downshift to -2.465 eV, which is close to that of Pt (111) (-2.687 eV). Additionally, the density of states (DOS) near the Fermi level of Pt in Pt SASs/AG catalyst is as large as that of the Pt in Pt (111), eventually promoted the HER activity.

Secondly, non-noble metal atoms such as transition metals are used to replace noble metals for preparing efficient HER catalysts, and even metal-free catalysts with excellent performance were designed and synthesized experimentally.[24, 126-130] For example, using the first principle DFT calculations, 3D, 4D, and 5D transition metal SACs in N-doped 2D graphene and nanographene of various sizes are screened for HER by Fung *et al*.[131] For most SACs, a *d*-band center downshift will occur when moving from graphene to nanographene, indicating that the hydrogen adsorption on metal SACs can be tuned by adjusting the size and dimension of the substrate. V, Rh, and Ir embedded on N-doped nanographene show much better HER activity than those on the extended 2D graphene. The machine learning models (kernel ridge regression, decision trees (random forest), and neural networks) and SISSO (Sure Independence Screening and Sparsifying Operator) method are employed to accurately predict the ΔG_H using various proposed descriptors, the results are shown in Figure 8 (a) to (d). Topological defect-based and complex defect-based carbon materials are also promising electrocatalysts. Yao and co-workers synthesized a series of defective carbons *via* a facile nitrogen removal procedure from N-doped graphene, and the edge-defect model called 7557-4 shows outstanding HER performance with the lowest calculated free energy of 0.187 eV (Figure 8 (g) and (h)).[16] DFT calculations were also performed to better understand the underlying catalytic mechanisms. The analysis of the frontier molecular orbitals shows that the catalytic activity of edge atoms is laid on their most

Preprints (www.preprints.org) | NOT PEER-REVIEWED | Posted: 23 November 2022 doi:10.20944/preprints202211.0444.v1

contribution to the highest occupied molecular orbital (HOMO) and lowest unoccupied molecular orbital (LUMO), which are highly correlated with the catalytic reactions (Figure 8 (e) and (f)).

4.2 Oxygen Evolution Reaction (OER) and Oxygen Reduction Reaction (ORR)

Oxygen evolution reaction (OER, $2H_2O\ (l) \rightarrow O_2\ (g) + 4e^- + 4H^+$) is the anode half-cell reaction of water splitting containing 4 electron transitions, as shown in Eq. 4.4. Oxygen reduction reaction (ORR, $O_2\ (g) + 4e^- + 4H^+ \rightarrow 2H_2O\ (l)$, Eq. 4.5) is the revise reaction of the OER, which is the cathodic reaction of fuel cells and zinc-air batteries.[132]

$$H_2O\ (l) + * \rightarrow OH^* + e^- + H^+ \quad \text{Eq. 4.4a}$$

$$OH^* \rightarrow O^* + e^- + H^+ \quad \text{Eq. 4.4b}$$

$$O^* + H_2O\ (l) \rightarrow OOH^* + e^- + H^+ \quad \text{Eq. 4.4c}$$

$$OOH^* \rightarrow O_2 + e^- + H^+ \quad \text{Eq. 4.4d}$$

$$O_2 + e^- + H^+ \rightarrow OOH^* \quad \text{Eq. 4.5a}$$

$$OOH^* + e^- + H^+ \rightarrow O^* + H_2O\ (l) \quad \text{Eq. 4.5b}$$

$$O^* + e^- + H^+ \rightarrow OH^* \quad \text{Eq. 4.5c}$$

$$OH^* + e^- + H^+ \rightarrow H_2O\ (l) + * \quad \text{Eq. 4.5d}$$

Both the OER and ORR are restricted by the slash kinetic and high reaction energy barriers, thus electrocatalysts are needed to accelerate the reaction rate and improve the efficiency. However, the high cost and low abundance of current commercial noble-metal-based catalysts, i.e., Pt/C for ORR, RuO_2 and IrO_2 for OER severely hinder their widespread applications. Similarly, the strategies of lowering the cost and improving the performance of the HER catalysts are also applicable to the OER and ORR electrocatalysts, and great achievements have been achieved.[60, 133-137] Zhang *et al.* anchored atomical distributed Ni atoms onto N-doped hollow carbon matrix (HCM@Ni-N).[138] In alkaline conditions, the HCM@Ni-N only requires

Preprints (www.preprints.org) | NOT PEER-REVIEWED | Posted: 23 November 2022 doi:10.20944/preprints202211.0444.v1

an OER overpotential of 304 mV to reach the current density of 10 mA cm^{-2}, which is much lower than that of the RuO_2 (393 mV), suggesting excellent OER activity of the prepared catalyst. Through the calculated distributions of charge density, they found that the electronic distribution of N-doped HCM was changed obviously after the Ni decoration (Figure 9a). At the same time, under the influence of Ni-N interaction, the *3d* orbital of Ni in HCM@Ni-N shows a leftward shift and the *d*-band center of the Ni was downshift from -0.94 eV to -2.04 eV (Figure 9b). According to the *d*-band center theory, this change could facilitate the desorption of adsorbates and reduce the energy barrier. The free energy pathways of the OER can also be calculated by DFT simulations and they are in good agreement with the experimental results (Figure 9c and d). By encapsulating Co and *β*-Mo_2C into N-doped carbon nanotubes (Co/*β*-Mo_2C@N-CNT), Ouyang and co-workers successfully fabricated a bifunctional electrocatalyst for the HER and OER in an alkaline electrolyte.[139] Based on the heterointerface between Co and *β*-Mo_2C, the OER activity of *β*-Mo_2C is enhanced significantly. With the assistance of DFT calculations, they proved that the cooperation of N-CNTs, Co and *β*-Mo_2C resulted in the low energy barriers of the intermediates, thus greatly improved the HER and OER kinetics.

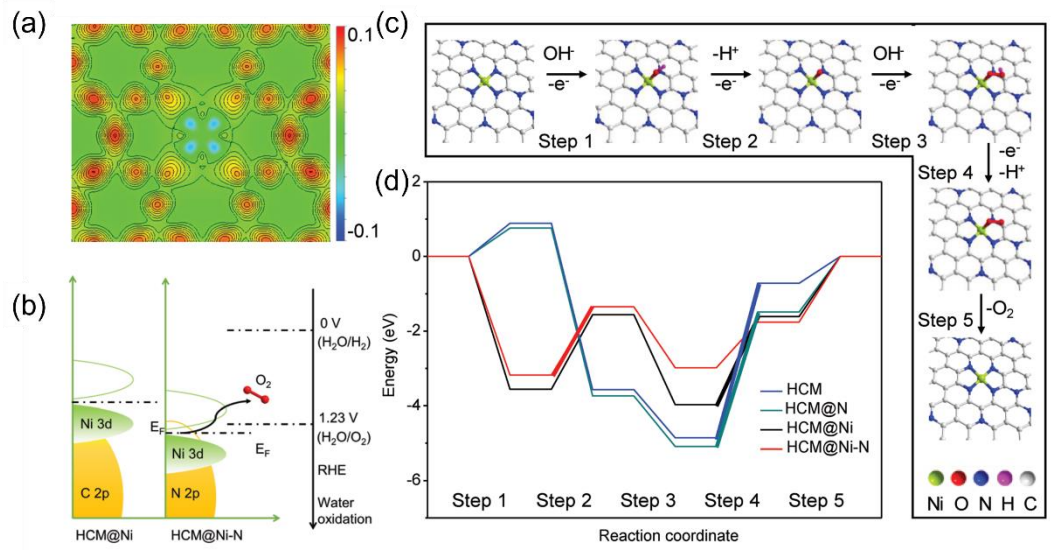

Figure 9. (a) Calculated distribution of charge density for HCM@Ni-N. (b) Schematic band diagrams of HCM@Ni and HCM@Ni-N. (c) Proposed mechanism of O_2 evolution over HCM@Ni-N. (d) Free energy diagram at 0 V for OER over HCM, HCM@N, HCM@Ni, and HCM@Ni-N. The bold lines indicate the rate-determining step. Reproduced with permission.[138] Copyright 2019, John Wiley and Sons.

 doi:10.20944/preprints202211.0444.v1

Under the guidance of DFT calculations, Wang *et al.* successfully synthesized a series of topological carbon defects through a facile N-removing strategy, among which adjacent pentagons (A-C5) show the best catalytic performance for the ORR and the edge divacancy defects (C585-2) are favourable for the HER.[140] DFT calculations were applied to investigate the relationship between the original carbon structure, the type of N configuration obtained, and the corresponding defect structures, for example, perfect carbon network versus graphitic-N versus C585 (Figure 10 a), edge-rich hexagonal structure versus pyridinic-N versus S-C5 (Figure 10 b), and edge-rich pentagon versus pyrrolic-N versus A-C5 (Figure 10 c). By a spontaneous gas-foaming method, Jiang and co-workers fabricated a range of promising trifunctional electrocatalysts called defect-rich N-doped ultrathin carbon nanosheets for HER, OER and ORR.[141] In rechargeable Zn-air batteries, NCN-1000-5 exhibits a high energy density (806 W h/kg), a low charge/recharge voltage gap (0.77 V) and extremely long cycle life (over 300 h). DFT calculations were used to identify the intrinsic active sites for the electrochemical reactions. The catalytic performance of various active sites for the ORR and OER were investigated, the results are shown in the volcano plot (Figure 10 d). The armchair edge carbon atoms, which are adjacent to the graphitic-N, possess the lowest overpotential, thus they should be the optimal catalytic active center for the specific electrocatalysis (Figure 10 e-g).

Preprints (www.preprints.org) | NOT PEER-REVIEWED | Posted: 23 November 2022 doi:10.20944/preprints202211.0444.v1

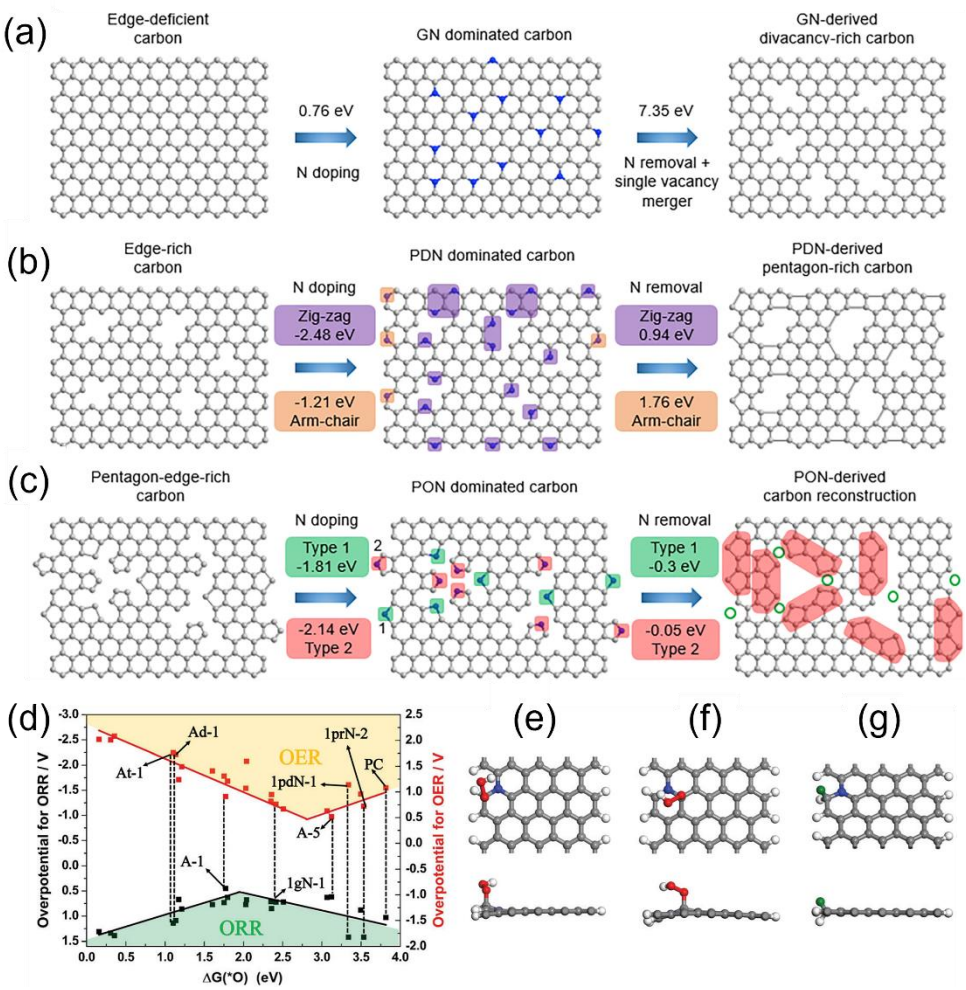

Figure 10. Computational simulation of specific N-doping and removing process in different carbon models: (a) Schematic and formation energy calculation of transformation from edge-deficient carbon to GN dominated carbon and then to divacancy-rich carbon. (b) Schematic and formation energy calculation of transformation from edge-rich carbon to PDN dominated carbon and then to pentagon-rich carbon. (c) Schematic and formation energy calculation of transformation from pentagon-edge-rich carbon to PON dominated carbon and then to special carbon reconstruction. Reproduced with permission.[140] Copyright 2020, Elsevier. (d) The volcano plot for the ORR and OER by plotting the overpotential as a function of $\Delta G(*O)$ at various possible active sites. The top and side views of the active site (e) A-1 for the ORR, (f) A-3 for the OER with OOH adsorbed, and (g) A-1 for the HER, the green ball representing the adsorbed H (θ = 2.27%). Reproduced with permission.[141] Copyright 2008, Royal Society of Chemistry.

Preprints (www.preprints.org) | NOT PEER-REVIEWED | Posted: 23 November 2022 doi:10.20944/preprints202211.0444.v1

4.3 Carbon Dioxide Reduction Reaction (CO_2RR)

Carbon dioxide reduction reaction (CO_2RR) could convert CO_2 to many value-added chemical compounds, such as CO, CH_4, CH_3OH, and C_2H_5OH (Eq. 4.6),[142, 143] which can be directly used as fuels to replace fossil fuels like gasoline and natural gas. Therefore, the CO_2RR may be regarded as the reverse reaction of the fossil fuel combustion and can significantly relief the greenhouse effect. However, the hydrogen atoms necessary for the reduction of CO_2 molecule are transported from the aqueous solution, so the HER must be considered as the competitive reaction. High cost of the currently used noble metal-based catalysts and the low selectivity of CO_2RR are still the biggest obstacle for its industrialization. Therefore, developing highly efficient and selective non-noble metal CO_2RR catalysts based on earth abundant elements has attracted the most attention in this promising research field.[144-149]

$$CO_2 + e^- \rightarrow CO_2^- \qquad E^\theta = -1.90\,V \qquad \text{Eq. 4.6a}$$

$$CO_2 + 2H^+ + 2e^- \rightarrow CO + H_2O \qquad E^\theta = -0.52\,V \qquad \text{Eq. 4.6b}$$

$$CO_2 + 2H^+ + 2e^- \rightarrow HCOOH \qquad E^\theta = -0.61\,V \qquad \text{Eq. 4.6c}$$

$$CO_2 + 4H^+ + 4e^- \rightarrow HCOH + H_2O \qquad E^\theta = -0.51\,V \qquad \text{Eq. 4.6d}$$

$$CO_2 + 6H^+ + 6e^- \rightarrow CH_3OH + H_2O \qquad E^\theta = -0.38\,V \qquad \text{Eq. 4.6e}$$

$$CO_2 + 8H^+ + 8e^- \rightarrow CH_4 + 2H_2O \qquad E^\theta = -0.24\,V \qquad \text{Eq. 4.6f}$$

$$CO_2 + 12H^+ + 12e^- \rightarrow C_2H_4 + 4H_2O \qquad E^\theta = -0.34\,V \qquad \text{Eq. 4.6g}$$

The initial stage of CO_2 reduction is CO_2 adsorption, which is crucial step of the CO_2RR. Zhu *et al.* systematically investigated the adsorption of CO_2 on g-C_3N_4 surface by DFT calculations.[150] Through analyzing the electronic properties such as the band gap, density of states, work function, HOMO and LUMO, they proved that the two-coordinated N atoms, which contributed to both valance band and conduction band edge, have the most negative adsorption energy (-0.4181) for CO_2 molecule. CO_2 can be effectively captured and activated on Si due to the "acceptance and back-donation" of electrons between the Si dopant and CO_2 molecule. Accordingly, Mao and co-workers designed an experimentally synthesizable electrocatalyst called silicon-doped graphene edges (Si chain@G).[151] The catalytic performance of the Si@ZZG (Si atoms doped into the zigzag edge of graphene) and Si@ACG (Si atoms

Preprints (www.preprints.org) | NOT PEER-REVIEWED | Posted: 23 November 2022 doi:10.20944/preprints202211.0444.v1

doped into the armchair edge of graphene) was exhaustively studied through DFT calculations (Figure 11a). CO_2 can be well captured and efficiently activated on Si@G, the binding energy at the zigzag and armchair edges is -0.65 eV and -0.83 eV, respectively. Remarkably, CO_2 can be converted to CH_3OH effectively when the Si@ACG was served as the active sites (Figure 11c). Moreover, Si chain@G with multiple Si active sites which are beneficial to product multiple-carbon productions was also investigated. They found that the Si chain@ZZG has a high selectivity to transform CO_2 to C_2H_5OH with an extreme low limiting potential of -0.6 V under the optimal theoretical reaction pathway (Figure 11b).

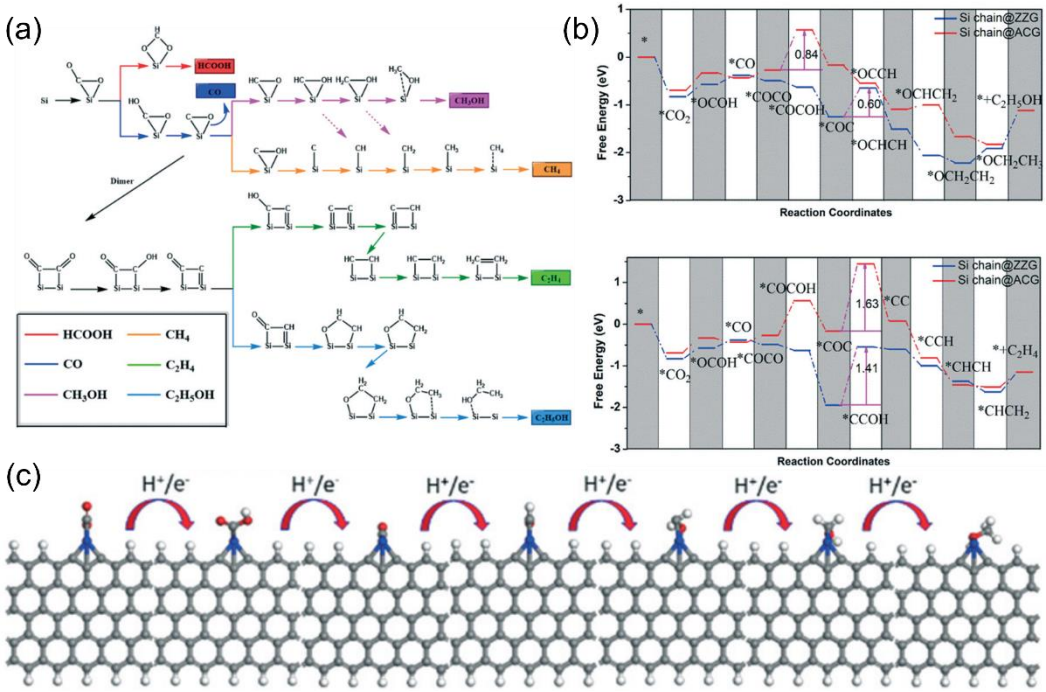

Figure 11. (a) Possible reaction pathways for the electrocatalytic reduction of CO_2 to six different products. (b) Gibbs free energy diagrams of CO_2 reduction reactions to CH_3OH and C_2H_4 on Si chain@ZZG and Si chain@ACG. (c) The optimised structures for CO_2 reduction to CH_3OH on the zigzag edge. Reproduced with permission.[151] Copyright 2011, Royal Society of Chemistry.

Transition metal atoms can also be excellent CO_2RR active centers. Guo *et al.* established calculation models with Fe, Co and Ni single atoms embedded onto graphitic carbon nitride (Fe/Co/Ni-C_3N_4) and systematically investigated the structures of the electrocatalysts, CO_2 adsorption configurations and the reduction mechanisms.[152] g-C_3N_4 with six-fold cavities was

Preprints (www.preprints.org) | NOT PEER-REVIEWED | Posted: 23 November 2022 doi:10.20944/preprints202211.0444.v1

selected as the substrate, the introduced Ni, Co, and Fe atoms are located from the corner to the center of the cavity. The PDOS of the metal *d* orbital and adsorbed CO_2 indicated that CO_2 could be chemically adsorbed on Co-C_3N_4 and Fe-C_3N_4, but physically adsorbed on Ni-C_3N_4 (Figure 12a and b). Guo also probed the reaction pathway and mechanism of different C1 products and thoroughly calculated the limiting potentials for the productions of CO, HCOOH, CH_3OH, and CH_4. They found that Co-C_3N_4 has superior CO_2RR activity and selectivity for CH_3OH (Figure 12c). Currently, copper (Cu) is found to be one of the best catalysts for achieving the high activity reduction of CO_2 to hydrocarbons since *CO_2 and *COOH can be effectively collected from Cu-based catalysts.[153] Due to the hydration of non-adsorbing CO_2 molecules, Pb, Hg, Cd, and Bi also demonstrate good catalytic performance for producing formate.[154] Other transition metals such as Ni, Fe, Pd, and Ti exhibit low CO_2RR selectivity because the HER is much favourable due to the strong H-bonding.[149]

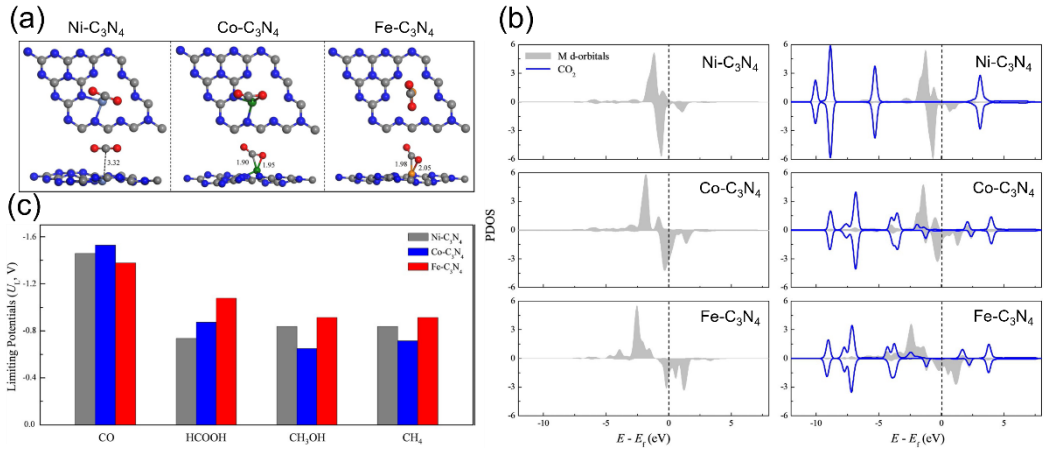

Figure 12. (a) The most stable CO_2 adsorption configurations. (b) PDOS of the metal *d* orbital before and after adsorption (including the adsorbent CO_2 total DOS). (c) Summary of the limiting potentials for the productions of CO, HCOOH, CH_3OH, and CH_4. Reproduced with permission.[152] Copyright 2019, John Wiley and Sons.

4.4 Nitrogen Reduction Reaction (NRR)

Nitrogen is the most abundant element in the earth and it is essential for all the organisms such as animals and plants. Ammonia (NH_3) is one of the most important industrial compounds due to its wide use in different fields. However, the ultra-stable N≡N triple bond greatly impedes the nitrogen fixation reaction. The industrial Haber-Bosch process uses N_2 and H_2 as the raw

Preprints (www.preprints.org) | NOT PEER-REVIEWED | Posted: 23 November 2022 doi:10.20944/preprints202211.0444.v1

materials, consuming excessive energy because of the high reaction temperature (350-550 °C) and pressure (150-350 atm).[155, 156] Therefore, the conversion of N_2 to NH_3 under ambient conditions is a promising research area. Recently, electrocatalytic nitrogen reduction reaction (NRR) has attracted increasingly research attentions because of its obvious advantages such as low energy consumption, reduced reaction temperature, and enhanced productivity.[157-164] Figure 13 shows the possible reaction pathways of the catalytic conversion of N_2 to NH_3.

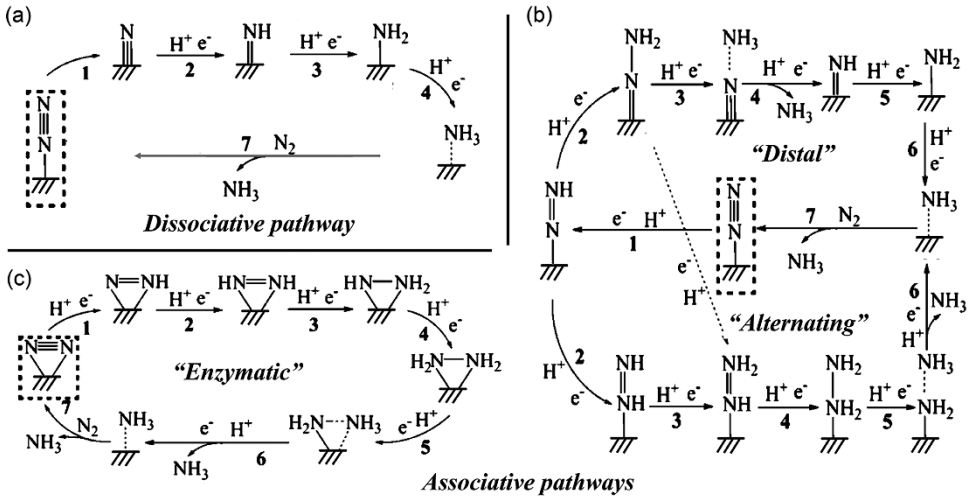

Figure 13. Schematic depiction of the dissociative pathways and the associative pathways (including distal, alternating, and enzymatic pathway) for catalytic conversion of N_2 to NH_3. Reproduced with permission.[157] Copyright 2016, American Chemical Society.

The first and also an important step of the NRR is the adsorption of N_2 to the active sites, which requires the atoms contain not fully occupied orbitals to accept the lone-pair electrons from the σ orbital of N_2. Therefore, transition metals would be excellent electron acceptors due to their half-occupied *d* orbitals and have the potential to be promising NRR electrocatalysts.[165-167] Ling and co-workers established a computational model which anchored Mo atoms onto N-doped carbon (Mo_1-N_1C_2) and investigated its NRR catalytic performance using the first principle calculations.[168] Firstly, the bonding energy of N_2 adsorbed on M_1-N_1C_2 (M = Cu, Pd, Pt, and Mo) is investigated, only Mo_1-N_1C_2 shows strong adsorption of N_2 with the adsorption energy of -1.19 and -1.18 eV for side-on and end-on adsorption, respectively. In addition, the N≡N bond length has increased from 1.12 Å (isolated N_2 molecule) to 1.18 Å (side-on) and 1.14 Å (end-on) (Figure 14 a-c). Accordingly, Mo is selected as the potential electrocatalyst, and the

Preprints (www.preprints.org) | NOT PEER-REVIEWED | Posted: 23 November 2022 doi:10.20944/preprints202211.0444.v1

possible reaction pathways are calculated. As shown in Figure 14 d, Mo_1-N_1C_2 has an extreme low overpotential of 0.24 V and can catalyze the NRR through an enzymatic pathway. It is worth noting that the generated NH_3 can be removed quickly from the Mo_1-N_1C_2 catalyst with a free-energy uphill of only 0.47 eV, which is significantly lower than that of the previously reported catalysts.

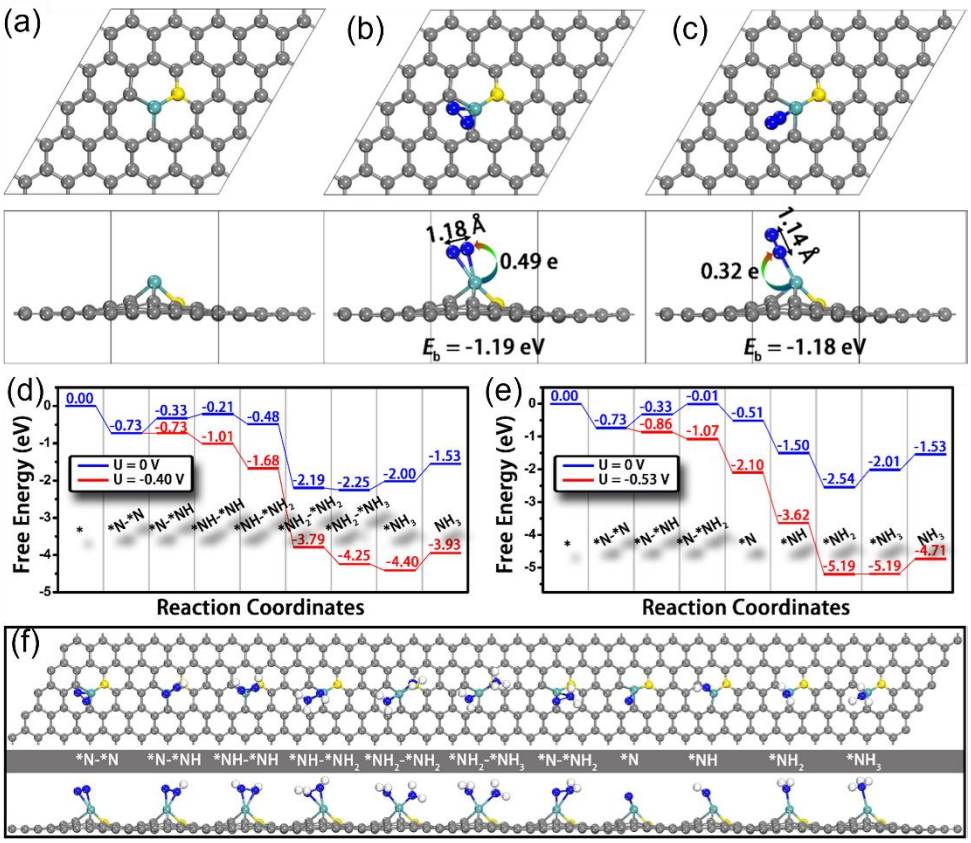

Figure 14. Top and side views of the structures of (a) Mo_1-N_1C_2, Mo_1-N_1C_2 with N_2 adsorption through (b) side-on and (c) end-on patterns. N−N bond lengths and charge transfer from Mo_1-N_1C_2 to N_2 are also presented. Free-energy diagrams for N_2 reduction through (d) enzymatic and (e) consecutive mechanisms at different applied potential as well as (f) the corresponding structures of the reaction intermediates. Gray, cyan, yellow, and blue balls represent the C, Mo, doped N, and adsorbed N atoms, respectively. Reproduced with permission.[168] Copyright 2018, American Chemical Society.

In recent years, metal-free catalysts have also emerged as an important category of electrocatalysts for ammonia formation. Boron (B) has the potential to be used in NRR

Preprints (www.preprints.org) | NOT PEER-REVIEWED | Posted: 23 November 2022 doi:10.20944/preprints202211.0444.v1

processes because of its Lewis acid-like characteristics and electron-deficient, which is different from other main group elements. The outer orbital of B undergoes hybridization to produce sp^2 orbitals, which can accept electron from the N_2 σ-bond and donate electron from the filled *2p* orbitals to the antibonding π^*-orbitals of N_2. This founding has been supported by a number of recent investigations.[169-171] For instance, Yu's group reported that B doped graphene could effectively catalyze the NRR with a very high Faradic efficiency of 10.8% for NH_3 production in aqueous solutions under ambient conditions at −0.5 V (versus RHE), with the electron redistribution at the active site constituting the reduction process.[171] However, the theoretically calculated overpotential remains very high, so there is still a great need for more suitable substrates to sustain B atoms. In addition, the detailed mechanism of the N_2 activation and reduction for non-metallic catalysts is yet to be uncovered, suggesting that new methods of nitrogen capture and activation should be exploited to increase the efficiency of the nitrogen fixation.

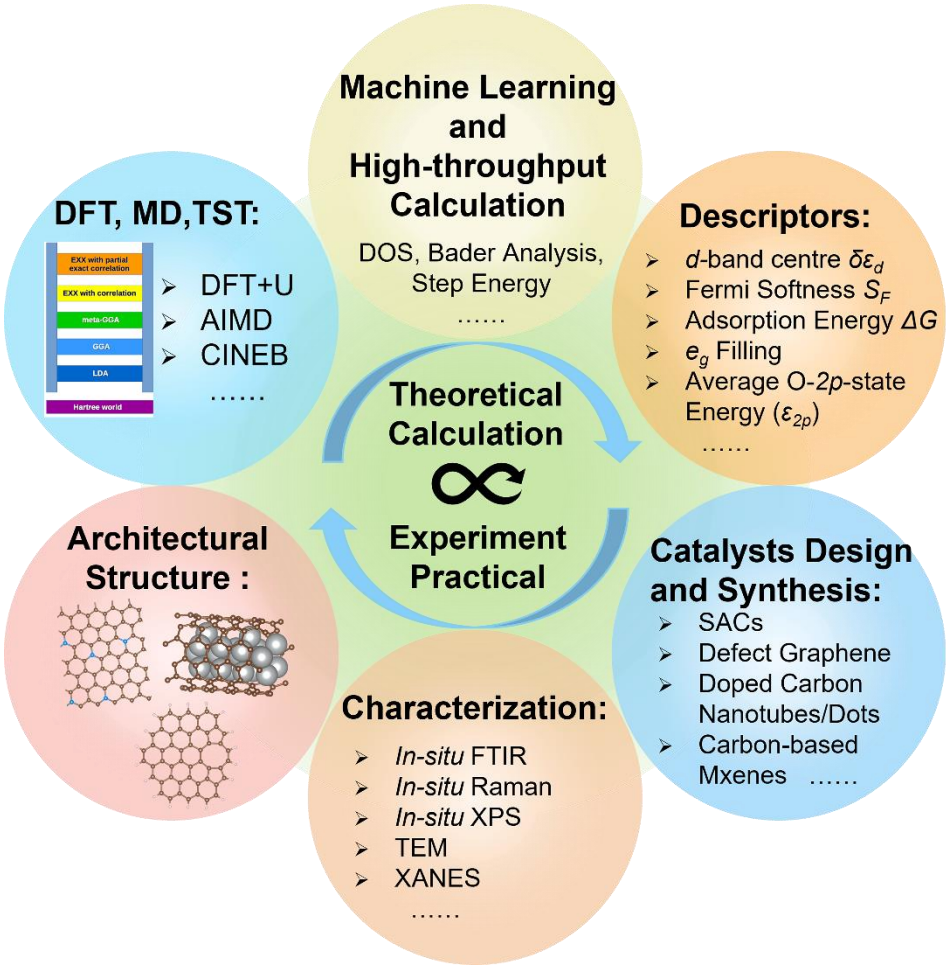

Figure 15. Schematic illustration showing the combination of theoretical calculations and experimental studies.

 doi:10.20944/preprints202211.0444.v1

5. Conclusions and Outlook

In summary, we have briefly introduced the development of modern DFT, and reviewed the application of theoretical calculations such as descriptors suit in material screening and mechanism investigating in carbon-based heterogeneous catalysts. Afterward, recent achievements of carbon-based electrocatalysts were presented. As shown in Figure 15, the development of supercomputer technology improves the accuracy of the theoretical calculations. With the assistance of machine learning and high-throughput computing, the prediction and screening ability of computational simulation has gradually enhanced and become more closely integrated with experimental work. Besides, DFT calculations can simulate more realistic reaction environment and material structures, which could improve the efficiency and accuracy of the mechanism explanation. Particularly, low-dimensional carbon-based materials have demonstrated a tremendous potential in the field of electrocatalysis due to their distinctive features, including 1) diverse and controllable structures as well as excellent environmental tolerance; 2) inherent substrate materials can be easily doped by heteroatoms; 3) various defects can serve as the active sites. However, severe limitations in the rational design and practical use of carbon-based electrocatalysts still exist. More universal, accurate and measurable descriptors should be developed, and additional research attention should be focused on the synthesis of catalysts. The following important issues and challenges deserve further investigations.

(1) Microkinetic modelling is a bridge that can connect quantum-chemical data with macroscopic behaviours in surface reactions. However, most attention has been focused on the analysis of the reaction energy and thermodynamics, more advancements in kinetic modelling are needed to fully comprehend the relationships between coverage, potential dependency of activation energies, adsorbate-adsorbate interactions, and pH effects.

(2) Existing theoretical approaches and functionals describing interface charge cannot meet the requirement of evaluating kinetics and reaction barriers of elementary steps under realistic reaction environments. For example, the widely used CHE model does not yet consider the non-electrochemical processes, proton-electron transfer, or the recombination of electrons and holes. For interfacial catalytic processes, multiscale modelling can facilitate the understanding of the transport effects.

 doi:10.20944/preprints202211.0444.v1

(3) The combination of multiple descriptors to effectively describe the relationship between structures and performance is required since it may be impossible to accurately predict the activity trends of complicated multi-phase catalysts only using one descriptor. Importantly, machine learning and high-throughput calculations should be valued to uncover more general descriptors and new reaction mechanisms.

(4) The synthesis of electrocatalysts with abundant active sites is also crucial, for instance, the formation process of specific defect structures, the synthesis of SACs with specific density are yet to be improved. Theoretical scientists have been focusing on improving the activity of electrocatalysts. However, rational design and synthesis strategies for large-scale production of carbon-based electrocatalysts are also one of the stumbling blocks for practical applications. More attention should be focused on the synthesis of electrocatalysts with targeted structural characteristics for a specific reaction.

(5) Scaling relationship between oxygen adsorbates in OER, ORR, and CO_2RR has the possibility to develop efficient descriptors. However, it also restricts the lowest overpotential of electrocatalytic reactions, for example, the predicted lowest overpotential is (3.2–2.46) eV/2e ≈ 0.4 V for both ORR and OER. Therefore, how to break the scaling relationship is also a prospective research topic in the near future.

Conflict of Interest

The authors declare no conflict of interest.

Acknowledgements

The authors would like to thank Australian Research Council (ARC DP200103043) for financial support during this work.

 doi:10.20944/preprints202211.0444.v1

References

1. Turner John, A., Sustainable Hydrogen Production. *Science* **2004,** *305* (5686), 972-974.
2. Dai, L.; Xue, Y.; Qu, L.; Choi, H.-J.; Baek, J.-B., Metal-Free Catalysts for Oxygen Reduction Reaction. *Chemical Reviews* **2015,** *115* (11), 4823-4892.
3. Gasteiger Hubert, A.; Marković Nenad, M., Just a Dream—or Future Reality? *Science* **2009,** *324* (5923), 48-49.
4. Abas, N.; Kalair, A.; Khan, N., Review of fossil fuels and future energy technologies. *Futures* **2015,** *69*, 31-49.
5. Chu, S.; Majumdar, A., Opportunities and challenges for a sustainable energy future. *Nature* **2012,** *488* (7411), 294-303.
6. Seh Zhi, W.; Kibsgaard, J.; Dickens Colin, F.; Chorkendorff, I.; Nørskov Jens, K.; Jaramillo Thomas, F., Combining theory and experiment in electrocatalysis: Insights into materials design. *Science* **2017,** *355* (6321), eaad4998.
7. Karunadasa, H. I.; Chang, C. J.; Long, J. R., A molecular molybdenum-oxo catalyst for generating hydrogen from water. *Nature* **2010,** *464* (7293), 1329-1333.
8. Liang, Y.; Li, Y.; Wang, H.; Dai, H., Strongly Coupled Inorganic/Nanocarbon Hybrid Materials for Advanced Electrocatalysis. *Journal of the American Chemical Society* **2013,** *135* (6), 2013-2036.
9. Zou, X.; Zhang, Y., Noble metal-free hydrogen evolution catalysts for water splitting. *Chemistry Society Review* **2015,** *44* (15), 5148-80.
10. Liu, M.; Zhao, Z.; Duan, X.; Huang, Y., Nanoscale Structure Design for High-Performance Pt-Based ORR Catalysts. *Advanced Materials* **2019,** *31* (6), 1802234.
11. Sui, S.; Wang, X.; Zhou, X.; Su, Y.; Riffat, S.; Liu, C.-j., A comprehensive review of Pt electrocatalysts for the oxygen reduction reaction: Nanostructure, activity, mechanism and carbon support in PEM fuel cells. *Journal of Materials Chemistry A* **2017,** *5* (5), 1808-1825.
12. Yan, Y.; Xia, B. Y.; Zhao, B.; Wang, X., A review on noble-metal-free bifunctional heterogeneous catalysts for overall electrochemical water splitting. *Journal of Materials Chemistry A* **2016,** *4* (45), 17587-17603.
13. Zhang, B.-W.; Yang, H.-L.; Wang, Y.-X.; Dou, S.-X.; Liu, H.-K., A Comprehensive Review

on Controlling Surface Composition of Pt-Based Bimetallic Electrocatalysts. *Advanced Energy Materials* **2018,** *8* (20), 1703597.

14. Mao, X.; Zhang, L.; Kour, G.; Zhou, S.; Wang, S.; Yan, C.; Zhu, Z.; Du, A., Defective Graphene on the Transition-Metal Surface: Formation of Efficient Bifunctional Catalysts for Oxygen Evolution/Reduction Reactions in Alkaline Media. *ACS Applied Materials & Interfaces* **2019,** *11* (19), 17410-17415.
15. Novoselov, K. S.; Geim, A. K.; Morozov, S. V.; Jiang, D.; Zhang, Y.; Dubonos, S. V.; Grigorieva, I. V.; Firsov, A. A., Electric Field Effect in Atomically Thin Carbon Films. *Science* **2004,** *306* (5696), 666-669.
16. Jia, Y.; Zhang, L.; Du, A.; Gao, G.; Chen, J.; Yan, X.; Brown, C. L.; Yao, X., Defect Graphene as a Trifunctional Catalyst for Electrochemical Reactions. *Advanced Materials* **2016,** *28* (43), 9532-9538.
17. Yan, X.; Jia, Y.; Chen, J.; Zhu, Z.; Yao, X., Defective-Activated-Carbon-Supported Mn–Co Nanoparticles as a Highly Efficient Electrocatalyst for Oxygen Reduction. *Advanced Materials* **2016,** *28* (39), 8771-8778.
18. Guo, Y.; Yuan, P.; Zhang, J.; Xia, H.; Cheng, F.; Zhou, M.; Li, J.; Qiao, Y.; Mu, S.; Xu, Q., Co_2P–CoN Double Active Centers Confined in N-Doped Carbon Nanotube: Heterostructural Engineering for Trifunctional Catalysis toward HER, ORR, OER, and Zn–Air Batteries Driven Water Splitting. *Advanced Functional Materials* **2018,** *28* (51), 1805641.
19. Chen, B.; Parker, G.; Han, J.; Meyyappan, M.; Cassell, A. M., Heterogeneous Single-Walled Carbon Nanotube Catalyst Discovery and Optimization. *Chemistry of Materials* **2002,** *14* (4), 1891-1896.
20. Hsieh, C.-T.; Lin, J.-Y.; Wei, J.-L., Deposition and electrochemical activity of Pt-based bimetallic nanocatalysts on carbon nanotube electrodes. *International Journal of Hydrogen Energy* **2009,** *34* (2), 685-693.
21. Chen, Y.; Wang, J.; Meng, X.; Zhong, Y.; Li, R.; Sun, X.; Ye, S.; Knights, S., Pt–SnO_2/nitrogen-doped CNT hybrid catalysts for proton-exchange membrane fuel cells (PEMFC): Effects of crystalline and amorphous SnO_2 by atomic layer deposition. *Journal of Power Sources* **2013,** *238*, 144-149.
22. Kroto, H. W.; Heath, J. R.; O'Brien, S. C.; Curl, R. F.; Smalley, R. E., C60:

Buckminsterfullerene. *Nature* **1985,** *318* (6042), 162-163.

23. Zhuo, J.; Wang, T.; Zhang, G.; Liu, L.; Gan, L.; Li, M., Salts of C60(OH)$_8$ Electrodeposited onto a Glassy Carbon Electrode: Surprising Catalytic Performance in the Hydrogen Evolution Reaction. *Angewandte Chemie International Edition* **2013,** *52* (41), 10867-10870.

24. He, T.; Gao, G.; Kou, L.; Will, G.; Du, A., Endohedral metallofullerenes (M@C60) as efficient catalysts for highly active hydrogen evolution reaction. *Journal of Catalysis* **2017,** *354*, 231-235.

25. Wu, J.; Ma, L.; Yadav, R. M.; Yang, Y.; Zhang, X.; Vajtai, R.; Lou, J.; Ajayan, P. M., Nitrogen-Doped Graphene with Pyridinic Dominance as a Highly Active and Stable Electrocatalyst for Oxygen Reduction. *ACS Applied Materials & Interfaces* **2015,** *7* (27), 14763-14769.

26. Liu, X.; Dai, L., Carbon-based metal-free catalysts. *Nature Reviews Materials* **2016,** *1* (11), 16064.

27. Liu, R.; Wu, D.; Feng, X.; Müllen, K., Nitrogen-Doped Ordered Mesoporous Graphitic Arrays with High Electrocatalytic Activity for Oxygen Reduction. *Angewandte Chemie International Edition* **2010,** *49* (14), 2565-2569.

28. Lin, Z.; Waller, G. H.; Liu, Y.; Liu, M.; Wong, C.-p., 3D Nitrogen-doped graphene prepared by pyrolysis of graphene oxide with polypyrrole for electrocatalysis of oxygen reduction reaction. *Nano Energy* **2013,** *2* (2), 241-248.

29. Bora, T.; Dousse, A.; Sharma, K.; Sarma, K.; Baev, A.; Hornyak, G. L.; Dasgupta, G., Modeling nanomaterial physical properties: theory and simulation. *International Journal of Smart and Nano Materials* **2019,** *10* (2), 116-143.

30. Thomas, L. H., The calculation of atomic fields. *Mathematical Proceedings of the Cambridge Philosophical Society* **1927,** *23* (5), 542-548.

31. E, F., Un metodo statistico per la determinazione di alcune priorieta dell'atome. *Rend. Accad. Naz. Lincei* **1927,** *6* (32).

32. Hohenberg, P.; Kohn, W., Inhomogeneous Electron Gas. *Physical Review* **1964,** *136* (3B), B864-B871.

33. Kohn, W.; Sham, L. J., Self-Consistent Equations Including Exchange and Correlation

Effects. *Physical Review* **1965,** *140* (4A), A1133-A1138.

34. Mattsson Ann, E., In Pursuit of the "Divine" Functional. *Science* **2002,** *298* (5594), 759-760.

35. Tao, J.; Perdew, J. P.; Staroverov, V. N.; Scuseria, G. E., Climbing the Density Functional Ladder: Nonempirical Meta--Generalized Gradient Approximation Designed for Molecules and Solids. *Physical Review Letters* **2003,** *91* (14), 146401.

36. Zhang, I. Y.; Xu, X., On the top rung of Jacob's ladder of density functional theory: Toward resolving the dilemma of SIE and NCE. *WIREs Computational Molecular Science* **2020,** *11* (1).

37. Becke, A. D., Density-functional exchange-energy approximation with correct asymptotic behavior. *Physical Review A* **1988,** *38* (6), 3098-3100.

38. Lee, C.; Yang, W.; Parr, R. G., Development of the Colle-Salvetti correlation-energy formula into a functional of the electron density. *Physical Review B* **1988,** *37* (2), 785-789.

39. White, J. A.; Bird, D. M., Implementation of gradient-corrected exchange-correlation potentials in Car-Parrinello total-energy calculations. *Physical Review B* **1994,** *50* (7), 4954-4957.

40. Perdew, J. P.; Chevary, J. A.; Vosko, S. H.; Jackson, K. A.; Pederson, M. R.; Singh, D. J.; Fiolhais, C., Atoms, molecules, solids, and surfaces: Applications of the generalized gradient approximation for exchange and correlation. *Physical Review B* **1992,** *46* (11), 6671-6687.

41. Perdew, J. P.; Burke, K.; Ernzerhof, M., Generalized Gradient Approximation Made Simple. *Physical Review Letters* **1996,** *77* (18), 3865-3868.

42. Zhao, Y.; Truhlar, D. G., Density Functionals with Broad Applicability in Chemistry. *Accounts of Chemical Research* **2008,** *41* (2), 157-167.

43. Zhao, Y.; Schultz, N. E.; Truhlar, D. G., Design of Density Functionals by Combining the Method of Constraint Satisfaction with Parametrization for Thermochemistry, Thermochemical Kinetics, and Noncovalent Interactions. *Journal of Chemical Theory and Computation* **2006,** *2* (2), 364-382.

44. Zhao, Y.; Truhlar, D. G., A new local density functional for main-group thermochemistry, transition metal bonding, thermochemical kinetics, and noncovalent interactions. *The*

 doi:10.20944/preprints202211.0444.v1

Journal of Chemical Physics **2006,** *125* (19), 194101.

45. Stephens, P. J.; Devlin, F. J.; Chabalowski, C. F.; Frisch, M. J., Ab Initio Calculation of Vibrational Absorption and Circular Dichroism Spectra Using Density Functional Force Fields. *The Journal of Physical Chemistry* **1994,** *98* (45), 5.
46. Heyd, J.; Scuseria, G. E., Efficient hybrid density functional calculations in solids: Assessment of the Heyd–Scuseria–Ernzerhof screened Coulomb hybrid functional. *The Journal of Chemical Physics* **2004,** *121* (3), 1187-1192.
47. Kresse, G.; Furthmüller, J., Efficiency of ab-initio total energy calculations for metals and semiconductors using a plane-wave basis set. *Computational Materials Science* **1996,** *6* (1), 15-50.
48. Kresse, G.; Furthmüller, J., Efficient iterative schemes for ab initio total-energy calculations using a plane-wave basis set. *Physical Review B* **1996,** *54* (16), 11169-11186.
49. Kresse, G.; Joubert, D., From ultrasoft pseudopotentials to the projector augmented-wave method. *Physical Review B* **1999,** *59* (3), 1758-1775.
50. Dudarev, S. L.; Botton, G. A.; Savrasov, S. Y.; Humphreys, C. J.; Sutton, A. P., Electron-energy-loss spectra and the structural stability of nickel oxide: An LSDA+U study. *Physical Review B* **1998,** *57* (3), 1505-1509.
51. Tolba, S. A.; Gameel, K. M.; Ali, B. A.; Almossalami, H. A.; Allam, N. K., The DFT+ U: Approaches, accuracy, and applications. *Density Functional Calculations-Recent Progresses of Theory and Application* **2018,** *1*, 5772.
52. Nosé, S., A unified formulation of the constant temperature molecular dynamics methods. *The Journal of Chemical Physics* **1984,** *81* (1), 511-519.
53. Hoover, W. G., Canonical dynamics: Equilibrium phase-space distributions. *Physical Review A* **1985,** *31* (3), 1695-1697.
54. Kresse, G.; Hafner, J., Ab initio molecular dynamics for liquid metals. *Physical Review B* **1993,** *47* (1), 558-561.
55. Henkelman, G.; Jónsson, H., A dimer method for finding saddle points on high dimensional potential surfaces using only first derivatives. *The Journal of Chemical Physics* **1999,** *111* (15), 7010-7022.
56. Henkelman, G.; Uberuaga, B. P.; Jónsson, H., A climbing image nudged elastic band

method for finding saddle points and minimum energy paths. *The Journal of Chemical Physics* **2000,** *113* (22), 9901-9904.

57. Zhou, S.; Yang, X.; Xu, X.; Dou, S. X.; Du, Y.; Zhao, J., Boron Nitride Nanotubes for Ammonia Synthesis: Activation by Filling Transition Metals. *J Am Chem Soc* **2020,** *142* (1), 308-317.

58. Sun, Y.; Cai, P.; Yang, D.; Yao, X., Single-site catalysis in heterogeneous electro-Fenton reaction for wastewater remediation. *Chem Catalysis* **2022,** *2* (4), 679-692.

59. Li, D.; Wang, B.; Long, X.; Xu, W.; Xia, Y.; Yang, D.; Yao, X., Controlled Asymmetric Charge Distribution of Active Centers in Conjugated Polymers for Oxygen Reduction. *Angewandte Chemie International Edition* **2021,** *60* (51), 26483-26488.

60. Yan, X.; Jia, Y.; Wang, K.; Jin, Z.; Dong, C.-L.; Huang, Y.-C.; Chen, J.; Yao, X., Controllable synthesis of Fe–N_4 species for acidic oxygen reduction. *Carbon Energy* **2020,** *2* (3), 452-460.

61. Wu, Q.; Jia, Y.; Liu, Q.; Mao, X.; Guo, Q.; Yan, X.; Zhao, J.; Liu, F.; Du, A.; Yao, X., Ultra-dense carbon defects as highly active sites for oxygen reduction catalysis. *Chem* **2022**, *8* (10), 2715-2733.

62. Tang, Y.; Yang, C.; Xu, X.; Kang, Y.; Henzie, J.; Que, W.; Yamauchi, Y., MXene Nanoarchitectonics: Defect-Engineered 2D MXenes towards Enhanced Electrochemical Water Splitting. *Advanced Energy Materials* **2022,** *12* (12), 2103867.

63. Wu, Y.; Wei, W.; Yu, R.; Xia, L.; Hong, X.; Zhu, J.; Li, J.; Lv, L.; Chen, W.; Zhao, Y.; Zhou, L.; Mai, L., Anchoring Sub-Nanometer Pt Clusters on Crumpled Paper-Like MXene Enables High Hydrogen Evolution Mass Activity. *Advanced Functional Materials* **2022,** *32* (17), 2110910.

64. Song, H.; Yu, J.; Tang, Z.; Yang, B.; Lu, S., Halogen-Doped Carbon Dots on Amorphous Cobalt Phosphide as Robust Electrocatalysts for Overall Water Splitting. *Advanced Energy Materials* **2022,** *12* (14), 2102573.

65. Ding, P.; Song, H.; Chang, J.; Lu, S., N-doped carbon dots coupled NiFe-LDH hybrids for robust electrocatalytic alkaline water and seawater oxidation. *Nano Research* **2022**.

66. Che, M., Nobel Prize in chemistry 1912 to Sabatier: Organic chemistry or catalysis? *Catalysis Today* **2013,** *218-219*, 162-171.

 doi:10.20944/preprints202211.0444.v1

67. Nørskov, J. K., Electronic factors in catalysis. *Progress in Surface Science* **1991,** *38* (2), 103-144.

68. Nilsson, A.; Pettersson, L. G. M.; Hammer, B.; Bligaard, T.; Christensen, C. H.; Nørskov, J. K., The electronic structure effect in heterogeneous catalysis. *Catalysis Letters* **2005,** *100* (3), 111-114.

69. Hammer, B.; Norskov, J. K., Why gold is the noblest of all the metals. *Nature* **1995,** *376* (6537), 238-240.

70. Kibler, L. A.; El-Aziz, A. M.; Hoyer, R.; Kolb, D. M., Tuning Reaction Rates by Lateral Strain in a Palladium Monolayer. *Angewandte Chemie International Edition* **2005,** *44* (14), 2080-2084.

71. Gao, R.; Pan, L.; Wang, H.; Zhang, X.; Wang, L.; Zou, J.-J., Ultradispersed Nickel Phosphide on Phosphorus-Doped Carbon with Tailored d-Band Center for Efficient and Chemoselective Hydrogenation of Nitroarenes. *ACS Catalysis* **2018,** *8* (9), 8420-8429.

72. Jiao, S.; Fu, X.; Huang, H., Descriptors for the Evaluation of Electrocatalytic Reactions: d-Band Theory and Beyond. *Advanced Functional Materials* **2022,** *32* (4), 2107651.

73. Tao, L.; Qiao, M.; Jin, R.; Li, Y.; Xiao, Z.; Wang, Y.; Zhang, N.; Xie, C.; He, Q.; Jiang, D.; Yu, G.; Li, Y.; Wang, S., Bridging the Surface Charge and Catalytic Activity of a Defective Carbon Electrocatalyst. *Angewandte Chemie International Edition* **2019,** *58* (4), 1019-1024.

74. Ye, L.; Ying, Y.; Sun, D.; Zhang, Z.; Fei, L.; Wen, Z.; Qiao, J.; Huang, H., Highly Efficient Porous Carbon Electrocatalyst with Controllable N-Species Content for Selective CO_2 Reduction. *Angewandte Chemie International Edition* **2020,** *59* (8), 3244-3251.

75. Wu, J.; Ma, S.; Sun, J.; Gold, J. I.; Tiwary, C.; Kim, B.; Zhu, L.; Chopra, N.; Odeh, I. N.; Vajtai, R.; Yu, A. Z.; Luo, R.; Lou, J.; Ding, G.; Kenis, P. J. A.; Ajayan, P. M., A metal-free electrocatalyst for carbon dioxide reduction to multi-carbon hydrocarbons and oxygenates. *Nature Communications* **2016,** *7* (1), 13869.

76. Deng, T.; Cen, C.; Shen, H.; Wang, S.; Guo, J.; Cai, S.; Deng, M., Atom-Pair Catalysts Supported by N-Doped Graphene for the Nitrogen Reduction Reaction: *d*-Band Center-Based Descriptor. *The Journal of Physical Chemistry Letters* **2020,** *11* (15), 6320-6329.

77. Zhou, S.; Yang, X.; Pei, W.; Liu, N.; Zhao, J., Heterostructures of MXenes and N-doped

graphene as highly active bifunctional electrocatalysts. *Nanoscale* **2018,** *10* (23), 10876-10883.

78. Huang, B.; Xiao, L.; Lu, J.; Zhuang, L., Spatially Resolved Quantification of the Surface Reactivity of Solid Catalysts. *Angewandte Chemie International Edition* **2016,** *55* (21), 6239-6243.

79. Gao, Z.; Sun, Y.; Li, M.; Yang, W.; Ding, X., Adsorption sensitivity of Fe decorated different graphene supports toward toxic gas molecules (CO and NO). *Applied Surface Science* **2018,** *456*, 351-359.

80. Yang, W.; Gao, Z.; Ding, X.; Lv, G.; Yan, W., The adsorption characteristics of mercury species on single atom iron catalysts with different graphene-based substrates. *Applied Surface Science* **2018,** *455*, 940-951.

81. Gao, Z. Y.; Yang, W. J.; Ding, X. L.; Lv, G.; Yan, W. P., Support effects on adsorption and catalytic activation of O_2 in single atom iron catalysts with graphene-based substrates. *Phys Chem Chem Phys* **2018,** *20* (10), 7333-7341.

82. Xiong, Y.; Dong, J.; Huang, Z.-Q.; Xin, P.; Chen, W.; Wang, Y.; Li, Z.; Jin, Z.; Xing, W.; Zhuang, Z.; Ye, J.; Wei, X.; Cao, R.; Gu, L.; Sun, S.; Zhuang, L.; Chen, X.; Yang, H.; Chen, C.; Peng, Q.; Chang, C.-R.; Wang, D.; Li, Y., Single-atom Rh/N-doped carbon electrocatalyst for formic acid oxidation. *Nature Nanotechnology* **2020,** *15* (5), 390-397.

83. Wang, B.; Zhang, F., Main Descriptors To Correlate Structures with the Performances of Electrocatalysts. *Angewandte Chemie International Edition* **2022,** *61* (4), e202111026.

84. Xie, T.; Wang, P.; Tian, C.; Zhao, G.; Jia, J.; He, C.; Zhao, C.; Wu, H., Adsorption Characteristics of Gas Molecules Adsorbed on Graphene Doped with Mn: A First Principle Study. *Molecules* **2022,** *27* (7).

85. Man, I. C.; Su, H.-Y.; Calle-Vallejo, F.; Hansen, H. A.; Martínez, J. I.; Inoglu, N. G.; Kitchin, J.; Jaramillo, T. F.; Nørskov, J. K.; Rossmeisl, J., Universality in Oxygen Evolution Electrocatalysis on Oxide Surfaces. *ChemCatChem* **2011,** *3* (7), 1159-1165.

86. J. K. Nørskov; T. Bligaard, a.; A. Logadottir, a.; J. R. Kitchin; J. G. Chen, b.; S. Pandelov, c.; and U. Stimmingc, Trends in the Exchange Current for Hydrogen Evolution. *Journal of The Electrochemical Society* **2005**.

87. Calle-Vallejo, F.; Loffreda, D.; Koper, M. T. M.; Sautet, P., Introducing structural

sensitivity into adsorption–energy scaling relations by means of coordination numbers. *Nature Chemistry* **2015,** *7* (5), 403-410.

88. Abild-Pedersen, F.; Greeley, J.; Studt, F.; Rossmeisl, J.; Munter, T. R.; Moses, P. G.; Skúlason, E.; Bligaard, T.; Nørskov, J. K., Scaling Properties of Adsorption Energies for Hydrogen-Containing Molecules on Transition-Metal Surfaces. *Physical Review Letters* **2007,** *99* (1), 016105.

89. Seh, Z. W.; Kibsgaard, J.; Dickens, C. F.; Chorkendorff, I.; Nørskov, J. K.; Jaramillo, T. F., Combining theory and experiment in electrocatalysis: Insights into materials design. *Science* **2017,** *355* (6321), eaad4998.

90. Zheng, Y.; Jiao, Y.; Qiao, S. Z., Engineering of Carbon-Based Electrocatalysts for Emerging Energy Conversion: From Fundamentality to Functionality. *Advanced Materials* **2015,** *27* (36), 5372-5378.

91. Mao, X.; Ling, C.; Tang, C.; Yan, C.; Zhu, Z.; Du, A., Predicting a new class of metal-organic frameworks as efficient catalyst for bi-functional oxygen evolution/reduction reactions. *Journal of Catalysis* **2018,** *367*, 206-211.

92. Ling, C.; Ouyang, Y.; Li, Q.; Bai, X.; Mao, X.; Du, A.; Wang, J., A General Two-Step Strategy–Based High-Throughput Screening of Single Atom Catalysts for Nitrogen Fixation. *Small Methods* **2018,** *3* (9).

93. Matsumoto, Y.; Yoneyama, H.; Tamura, H., Catalytic activity for electrochemical reduction of oxygen of lanthanum nickel oxide and related oxides. *Journal of Electroanalytical Chemistry and Interfacial Electrochemistry* **1977,** *79* (2), 319-326.

94. Matsumoto, Y.; Yoneyama, H.; Tamura, H., Influence of the nature of the conduction band of transition metal oxides on catalytic activity for oxygen reduction. *Journal of Electroanalytical Chemistry and Interfacial Electrochemistry* **1977,** *83* (2), 237-243.

95. Lee, Y.-L.; Kleis, J.; Rossmeisl, J.; Shao-Horn, Y.; Morgan, D., Prediction of solid oxide fuel cell cathode activity with first-principles descriptors. *Energy & Environmental Science* **2011,** *4* (10).

96. Grimaud, A.; May, K. J.; Carlton, C. E.; Lee, Y.-L.; Risch, M.; Hong, W. T.; Zhou, J.; Shao-Horn, Y., Double perovskites as a family of highly active catalysts for oxygen evolution in alkaline solution. *Nature Communications* **2013,** *4* (1), 2439.

97. Chattot, R.; Le Bacq, O.; Beermann, V.; Kühl, S.; Herranz, J.; Henning, S.; Kühn, L.; Asset, T.; Guétaz, L.; Renou, G.; Drnec, J.; Bordet, P.; Pasturel, A.; Eychmüller, A.; Schmidt, T. J.; Strasser, P.; Dubau, L.; Maillard, F., Surface distortion as a unifying concept and descriptor in oxygen reduction reaction electrocatalysis. *Nature Materials* **2018,** *17* (9), 827-833.

98. Calle-Vallejo, F.; Martínez, J. I.; García-Lastra, J. M.; Sautet, P.; Loffreda, D., Fast Prediction of Adsorption Properties for Platinum Nanocatalysts with Generalized Coordination Numbers. *Angewandte Chemie International Edition* **2014,** *53* (32), 8316-8319.

99. Calle-Vallejo, F.; Tymoczko, J.; Colic, V.; Vu Quang, H.; Pohl Marcus, D.; Morgenstern, K.; Loffreda, D.; Sautet, P.; Schuhmann, W.; Bandarenka Aliaksandr, S., Finding optimal surface sites on heterogeneous catalysts by counting nearest neighbors. *Science* **2015,** *350* (6257), 185-189.

100. Wan, X.; Zhang, Z.; Niu, H.; Yin, Y.; Kuai, C.; Wang, J.; Shao, C.; Guo, Y., Machine-Learning-Accelerated Catalytic Activity Predictions of Transition Metal Phthalocyanine Dual-Metal-Site Catalysts for CO_2 Reduction. *The Journal of Physical Chemistry Letters* **2021,** *12* (26), 6111-6118.

101. Tran, K.; Ulissi, Z. W., Active learning across intermetallics to guide discovery of electrocatalysts for CO_2 reduction and H_2 evolution. *Nature Catalysis* **2018,** *1* (9), 696-703.

102. Guo, X.; Lin, S.; Gu, J.; Zhang, S.; Chen, Z.; Huang, S., Simultaneously Achieving High Activity and Selectivity toward Two-Electron O_2 Electroreduction: The Power of Single-Atom Catalysts. *ACS Catalysis* **2019,** *9* (12), 11042-11054.

103. Mao, X.; Wang, L.; Xu, Y.; Wang, P.; Li, Y.; Zhao, J., Computational high-throughput screening of alloy nanoclusters for electrocatalytic hydrogen evolution. *npj Computational Materials* **2021,** *7* (1), 46.

104. Guan, D.; Zhou, J.; Hu, Z.; Zhou, W.; Xu, X.; Zhong, Y.; Liu, B.; Chen, Y.; Xu, M.; Lin, H.-J.; Chen, C.-T.; Wang, J.-Q.; Shao, Z., Searching General Sufficient-and-Necessary Conditions for Ultrafast Hydrogen-Evolving Electrocatalysis. *Advanced Functional Materials* **2019,** *29* (20), 1900704.

105. Parker, A. J.; Opletal, G.; Barnard, A. S., Classification of platinum nanoparticle catalysts using machine learning. *Journal of Applied Physics* **2020,** *128* (1), 014301.

106. Back, S.; Tran, K.; Ulissi, Z. W., Toward a Design of Active Oxygen Evolution Catalysts: Insights from Automated Density Functional Theory Calculations and Machine Learning. *ACS Catalysis* **2019,** *9* (9), 7651-7659.

107. Wexler, R. B.; Martirez, J. M. P.; Rappe, A. M., Chemical Pressure-Driven Enhancement of the Hydrogen Evolving Activity of Ni_2P from Nonmetal Surface Doping Interpreted via Machine Learning. *Journal of the American Chemical Society* **2018,** *140* (13), 4678-4683.

108. Zheng, J.; Sun, X.; Qiu, C.; Yan, Y.; Yao, Z.; Deng, S.; Zhong, X.; Zhuang, G.; Wei, Z.; Wang, J., High-Throughput Screening of Hydrogen Evolution Reaction Catalysts in MXene Materials. *The Journal of Physical Chemistry C* **2020,** *124* (25), 13695-13705.

109. Zhu, X.; Yan, J.; Gu, M.; Liu, T.; Dai, Y.; Gu, Y.; Li, Y., Activity Origin and Design Principles for Oxygen Reduction on Dual-Metal-Site Catalysts: A Combined Density Functional Theory and Machine Learning Study. *The Journal of Physical Chemistry Letters* **2019,** *10* (24), 7760-7766.

110. Zhang, N.; Yang, B.; Liu, K.; Li, H.; Chen, G.; Qiu, X.; Li, W.; Hu, J.; Fu, J.; Jiang, Y.; Liu, M.; Ye, J., Machine Learning in Screening High Performance Electrocatalysts for CO_2 Reduction. *Small Methods* **2021,** *5* (11), 2100987.

111. Hu, C.; Hu, Y.; Fan, C.; Yang, L.; Zhang, Y.; Li, H.; Xie, W., Surface-Enhanced Raman Spectroscopic Evidence of Key Intermediate Species and Role of NiFe Dual-Catalytic Center in Water Oxidation. *Angewandte Chemie (International ed. in English)* **2021,** *60* (36), 19774-19778.

112. Khan, K.; Liu, T.; Arif, M.; Yan, X.; Hossain, M. D.; Rehman, F.; Zhou, S.; Yang, J.; Sun, C.; Bae, S.-H.; Kim, J.; Amine, K.; Pan, X.; Luo, Z., Laser-Irradiated Holey Graphene-Supported Single-Atom Catalyst towards Hydrogen Evolution and Oxygen Reduction. *Advanced Energy Materials* **2021,** *11* (40), 2101619.

113. Lan, J.; Luo, M.; Han, J.; Peng, M.; Duan, H.; Tan, Y., Nanoporous $B_{13}C_2$ towards Highly Efficient Electrochemical Nitrogen Fixation. *Small* **2021,** *17* (39), 2102814.

114. Liu, Y.; Xue, Y.; Hui, L.; Yu, H.; Fang, Y.; He, F.; Li, Y., Porous graphdiyne loading CoO_x quantum dots for fixation nitrogen reaction. *Nano Energy* **2021,** *89*, 106333.

115. Zhang, L.; Fischer, J. M. T. A.; Jia, Y.; Yan, X.; Xu, W.; Wang, X.; Chen, J.; Yang, D.; Liu, H.; Zhuang, L.; Hankel, M.; Searles, D. J.; Huang, K.; Feng, S.; Brown, C. L.; Yao, X., Coordination of Atomic Co–Pt Coupling Species at Carbon Defects as Active Sites for

Oxygen Reduction Reaction. *Journal of the American Chemical Society* **2018,** *140* (34), 10757-10763.

116. Li, W.; Liu, Y.; Wu, M.; Feng, X.; Redfern, S. A. T.; Shang, Y.; Yong, X.; Feng, T.; Wu, K.; Liu, Z.; Li, B.; Chen, Z.; Tse, J. S.; Lu, S.; Yang, B., Carbon-Quantum-Dots-Loaded Ruthenium Nanoparticles as an Efficient Electrocatalyst for Hydrogen Production in Alkaline Media. *Advanced Materials* **2018,** *30* (31), e1800676.

117. Andreadis, G.; Tsiakaras, P., Ethanol crossover and direct ethanol PEM fuel cell performance modeling and experimental validation. *Chemical Engineering Science* **2006,** *61* (22), 7497-7508.

118. Hao, Y.; Wang, X.; Shen, J.; Yuan, J.; Wang, A.-J.; Niu, L.; Huang, S., One-pot synthesis of single-crystal Pt nanoplates uniformly deposited on reduced graphene oxide, and their high activity and stability on the electrocalalytic oxidation of methanol. *Nanotechnology* **2016,** *27* (14), 145602.

119. Yang, X.-F.; Wang, A.; Qiao, B.; Li, J.; Liu, J.; Zhang, T., Single-Atom Catalysts: A New Frontier in Heterogeneous Catalysis. *Accounts of Chemical Research* **2013,** *46* (8), 1740-1748.

120. Sun, S.; Zhang, G.; Gauquelin, N.; Chen, N.; Zhou, J.; Yang, S.; Chen, W.; Meng, X.; Geng, D.; Banis, M. N.; Li, R.; Ye, S.; Knights, S.; Botton, G. A.; Sham, T.-K.; Sun, X., Single-atom Catalysis Using Pt/Graphene Achieved through Atomic Layer Deposition. *Scientific Reports* **2013,** *3* (1), 1775.

121. Li, M.; Zhu, Y.; Song, N.; Wang, C.; Lu, X., Fabrication of Pt nanoparticles on nitrogen-doped carbon/Ni nanofibers for improved hydrogen evolution activity. *Journal of Colloid and Interface Science* **2018,** *514*, 199-207.

122. Ren, X.; Lv, Q.; Liu, L.; Liu, B.; Wang, Y.; Liu, A.; Wu, G., Current progress of Pt and Pt-based electrocatalysts used for fuel cells. *Sustainable Energy & Fuels* **2020,** *4* (1), 15-30.

123. Yang, Q.; Liu, H.; Yuan, P.; Jia, Y.; Zhuang, L.; Zhang, H.; Yan, X.; Liu, G.; Zhao, Y.; Liu, J.; Wei, S.; Song, L.; Wu, Q.; Ge, B.; Zhang, L.; Wang, K.; Wang, X.; Chang, C.-R.; Yao, X., Single Carbon Vacancy Traps Atomic Platinum for Hydrogen Evolution Catalysis. *Journal of the American Chemical Society* **2022,** *144* (5), 2171-2178.

124. Gao, G.; Bottle, S.; Du, A., Understanding the activity and selectivity of single atom catalysts for hydrogen and oxygen evolution via ab initial study. *Catalysis Science &*

Technology **2018,** *8* (4), 996-1001.

125. Ye, S.; Luo, F.; Zhang, Q.; Zhang, P.; Xu, T.; Wang, Q.; He, D.; Guo, L.; Zhang, Y.; He, C.; Ouyang, X.; Gu, M.; Liu, J.; Sun, X., Highly stable single Pt atomic sites anchored on aniline-stacked graphene for hydrogen evolution reaction. *Energy & Environmental Science* **2019,** *12* (3), 1000-1007.

126. Fan, L.; Liu, P. F.; Yan, X.; Gu, L.; Yang, Z. Z.; Yang, H. G.; Qiu, S.; Yao, X., Atomically isolated nickel species anchored on graphitized carbon for efficient hydrogen evolution electrocatalysis. *Nature Communications* **2016,** *7* (1), 10667.

127. Zhang, L.; Jia, Y.; Yan, X.; Yao, X., Activity Origins in Nanocarbons for the Electrocatalytic Hydrogen Evolution Reaction. *Small* **2018,** *14* (26), 1800235.

128. Ahsan, M. A.; He, T.; Eid, K.; Abdullah, A. M.; Curry, M. L.; Du, A.; Puente Santiago, A. R.; Echegoyen, L.; Noveron, J. C., Tuning the Intermolecular Electron Transfer of Low-Dimensional and Metal-Free BCN/C60 Electrocatalysts via Interfacial Defects for Efficient Hydrogen and Oxygen Electrochemistry. *Journal of the American Chemical Society* **2021,** *143* (2), 1203-1215.

129. He, T.; Zhang, C.; Du, A., Single-atom supported on graphene grain boundary as an efficient electrocatalyst for hydrogen evolution reaction. *Chemical Engineering Science* **2019,** *194*, 58-63.

130. Yasin, G.; Ibraheem, S.; Ali, S.; Arif, M.; Ibrahim, S.; Iqbal, R.; Kumar, A.; Tabish, M.; Mushtaq, M. A.; Saad, A.; Xu, H.; Zhao, W., Defects-engineered tailoring of tri-doped interlinked metal-free bifunctional catalyst with lower gibbs free energy of OER/HER intermediates for overall water splitting. *Materials Today Chemistry* **2022,** *23*, 100634.

131. Fung, V.; Hu, G.; Wu, Z.; Jiang, D.-e., Descriptors for Hydrogen Evolution on Single Atom Catalysts in Nitrogen-Doped Graphene. *The Journal of Physical Chemistry C* **2020,** *124* (36), 19571-19578.

132. Gasteiger, H. A.; Kocha, S. S.; Sompalli, B.; Wagner, F. T., Activity benchmarks and requirements for Pt, Pt-alloy, and non-Pt oxygen reduction catalysts for PEMFCs. *Applied Catalysis B: Environmental* **2005,** *56* (1), 9-35.

133. Yan, X.; Zhuang, L.; Zhu, Z.; Yao, X., Defect engineering and characterization of active sites for efficient electrocatalysis. *Nanoscale* **2021,** *13* (6), 3327-3345.

134. Yang, Q.; Jia, Y.; Wei, F.; Zhuang, L.; Yang, D.; Liu, J.; Wang, X.; Lin, S.; Yuan, P.; Yao, X., Understanding the Activity of Co-$N_{4-x}C_x$ in Atomic Metal Catalysts for Oxygen Reduction Catalysis. *Angewandte Chemie International Edition* **2020,** *59* (15), 6122-6127.

135. Wang, X.; Jia, Y.; Mao, X.; Liu, D.; He, W.; Li, J.; Liu, J.; Yan, X.; Chen, J.; Song, L.; Du, A.; Yao, X., Edge-Rich Fe−N_4 Active Sites in Defective Carbon for Oxygen Reduction Catalysis. *Advanced Materials* **2020,** *32* (16), 2000966.

136. He, T.; Zhang, C.; Will, G.; Du, A., Cobalt porphyrin supported on graphene/Ni (111) surface: Enhanced oxygen evolution/reduction reaction and the role of electron coupling. *Catalysis Today* **2020,** *351*, 113-118.

137. Zhu, M.; Zhou, Y.; Sun, Y.; Zhu, C.; Hu, L.; Gao, J.; Huang, H.; Liu, Y.; Kang, Z., Cobalt phosphide/carbon dots composite as an efficient electrocatalyst for oxygen evolution reaction. *Dalton Trans* **2018,** *47* (15), 5459-5464.

138. Zhang, H.; Liu, Y.; Chen, T.; Zhang, J.; Zhang, J.; Lou, X. W. D., Unveiling the Activity Origin of Electrocatalytic Oxygen Evolution over Isolated Ni Atoms Supported on a N-Doped Carbon Matrix. *Adv Mater* **2019,** *31* (48), e1904548.

139. Ouyang, T.; Ye, Y. Q.; Wu, C. Y.; Xiao, K.; Liu, Z. Q., Heterostructures Composed of N-Doped Carbon Nanotubes Encapsulating Cobalt and beta-Mo_2C Nanoparticles as Bifunctional Electrodes for Water Splitting. *Angew Chem Int Ed Engl* **2019,** *58* (15), 4923-4928.

140. Wang, X.; Jia, Y.; Mao, X.; Zhang, L.; Liu, D.; Song, L.; Yan, X.; Chen, J.; Yang, D.; Zhou, J.; Wang, K.; Du, A.; Yao, X., A Directional Synthesis for Topological Defect in Carbon. *Chem* **2020,** *6* (8), 2009-2023.

141. Jiang, H.; Gu, J.; Zheng, X.; Liu, M.; Qiu, X.; Wang, L.; Li, W.; Chen, Z.; Ji, X.; Li, J., Defect-rich and ultrathin N doped carbon nanosheets as advanced trifunctional metal-free electrocatalysts for the ORR, OER and HER. *Energy & Environmental Science* **2019,** *12* (1), 322-333.

142. Whipple, D. T.; Kenis, P. J. A., Prospects of CO_2 Utilization via Direct Heterogeneous Electrochemical Reduction. *The Journal of Physical Chemistry Letters* **2010,** *1* (24), 3451-3458.

143. Chen, J.; Wang, T.; Li, Z.; Yang, B.; Zhang, Q.; Lei, L.; Feng, P.; Hou, Y., Recent progress and perspective of electrochemical CO_2 reduction towards C2-C5 products over non-

precious metal heterogeneous electrocatalysts. *Nano Research* **2021,** *14* (9), 3188-3207.

144. He, T.; Zhang, L.; Kour, G.; Du, A., Electrochemical reduction of carbon dioxide on precise number of Fe atoms anchored graphdiyne. *Journal of CO_2 Utilization* **2020,** *37*, 272-277.

145. Mao, X.; Wijethunge, D.; Zhang, L.; Wang, S.; Yan, C.; Zhu, Z.; Du, A., Metal-free graphene/boron nitride heterointerface for CO_2 reduction: Surface curvature controls catalytic activity and selectivity. *EcoMat* **2020,** *2* (1), e12013.

146. Er, C.-C.; Tang, J.-Y.; Fung, C.-M.; Tan, L.-L.; Medhekar, N. V.; Chai, S.-P., Atomistic Insights into the Reformation of CH_4 with CO_2 on Metal-Free gC_3N_4: Unraveling the Reaction Mechanisms Using First-Principles DFT Calculations. *The Journal of Physical Chemistry C* **2021,** *125* (42), 23021-23028.

147. Powar, N. S.; Hiragond, C. B.; Bae, D.; In, S.-I., Two-dimensional metal carbides for electro- and photocatalytic CO_2 reduction: Review. *Journal of CO_2 Utilization* **2022,** *55*, 101814.

148. Zha, W.; Liu, D.; Ma, Z.; Wang, Y.; Wei, Y.; Ma, X.; Wang, L.; Zhang, Q.; Lou, B.; Yuan, R.; Fu, X.; Sa, R., Efficient electrochemical CO_2 reduction on C_2N monolayer supported transition metals trimer catalysts: A DFT study. *Applied Surface Science* **2021,** *564*, 150331.

149. Back, S.; Lim, J.; Kim, N. Y.; Kim, Y. H.; Jung, Y., Single-atom catalysts for CO_2 electroreduction with significant activity and selectivity improvements. *Chem Sci* **2017,** *8* (2), 1090-1096.

150. Zhu, B.; Zhang, L.; Xu, D.; Cheng, B.; Yu, J., Adsorption investigation of CO_2 on g-C_3N_4 surface by DFT calculation. *Journal of CO_2 Utilization* **2017,** *21*, 327-335.

151. Mao, X.; Kour, G.; Zhang, L.; He, T.; Wang, S.; Yan, C.; Zhu, Z.; Du, A., Silicon-doped graphene edges: an efficient metal-free catalyst for the reduction of CO_2 into methanol and ethanol. *Catalysis Science & Technology* **2019,** *9* (23), 6800-6807.

152. Guo, C.; Zhang, T.; Deng, X.; Liang, X.; Guo, W.; Lu, X.; Wu, C. L., Electrochemical CO_2 Reduction to C1 Products on Single Nickel/Cobalt/Iron-Doped Graphitic Carbon Nitride: A DFT Study. *ChemSusChem* **2019,** *12* (23), 5126-5132.

153. Raciti, D.; Wang, C., Recent Advances in CO_2 Reduction Electrocatalysis on Copper. *ACS Energy Letters* **2018,** *3* (7), 1545-1556.

154. Mao, X.; Tang, C.; He, T.; Wijethunge, D.; Yan, C.; Zhu, Z.; Du, A., Computational screening of MN_4 (M = Ti-Cu) based metal organic frameworks for CO_2 reduction using the *d*-band centre as a descriptor. *Nanoscale* **2020,** *12* (10), 6188-6194.

155. Chen Jingguang, G.; Crooks Richard, M.; Seefeldt Lance, C.; Bren Kara, L.; Bullock, R. M.; Darensbourg Marcetta, Y.; Holland Patrick, L.; Hoffman, B.; Janik Michael, J.; Jones Anne, K.; Kanatzidis Mercouri, G.; King, P.; Lancaster Kyle, M.; Lymar Sergei, V.; Pfromm, P.; Schneider William, F.; Schrock Richard, R., Beyond fossil fuel–driven nitrogen transformations. *Science* **2018,** *360* (6391), eaar6611.

156. van der Ham, C. J.; Koper, M. T.; Hetterscheid, D. G., Challenges in reduction of dinitrogen by proton and electron transfer. *Chem Soc Rev* **2014,** *43* (15), 5183-91.

157. Li, X.-F.; Li, Q.-K.; Cheng, J.; Liu, L.; Yan, Q.; Wu, Y.; Zhang, X.-H.; Wang, Z.-Y.; Qiu, Q.; Luo, Y., Conversion of Dinitrogen to Ammonia by FeN3-Embedded Graphene. *Journal of the American Chemical Society* **2016,** *138* (28), 8706-8709.

158. Cui, X.; Tang, C.; Zhang, Q., A Review of Electrocatalytic Reduction of Dinitrogen to Ammonia under Ambient Conditions. *Advanced Energy Materials* **2018,** *8* (22).

159. He, T.; Puente Santiago, A. R.; Du, A., Atomically embedded asymmetrical dual-metal dimers on N-doped graphene for ultra-efficient nitrogen reduction reaction. *Journal of Catalysis* **2020,** *388*, 77-83.

160. Wang, F.; Mao, J., Effect of N-doping on graphene: NRR activity and N-source. *Diamond and Related Materials* **2021,** *118*, 108494.

161. Liu, A.; Yang, Y.; Kong, D.; Ren, X.; Gao, M.; Liang, X.; Yang, Q.; Zhang, J.; Gao, L.; Ma, T., DFT study of the defective carbon materials with vacancy and heteroatom as catalyst for NRR. *Applied Surface Science* **2021,** *536*, 147851.

162. Samal, P. P.; Poonam; Krishnamurty, S., Substrate augmented catalytic activity towards NRR: A case study of Li doped Al clusters on defective graphene. *Applied Surface Science* **2021,** *566*, 150586.

163. Zhou, Y.; Wei, B.; Cao, H.; An, Z.; Li, M.; Huo, Y.; Jiang, J.; Jin, Z.; Xie, J.; He, M., Electroreduction of nitrogen to ammonia by single-atom catalysis with synergistic boron-carbon nitrogen nanotubes. *Journal of Environmental Chemical Engineering* **2022,** *10* (3), 107752.

 doi:10.20944/preprints202211.0444.v1

164. Ruiyi, L.; Keyang, H.; Pengwu, X.; Wendong, W.; Nana, L.; Haiyan, Z.; Zaijun, L.; Xiaohao, L., Synthesis of a ruthenium–graphene quantum dot–graphene hybrid as a promising single-atom catalyst for electrochemical nitrogen reduction with ultrahigh yield rate and selectivity. *Journal of Materials Chemistry A* **2021,** *9* (43), 24582-24589.

165. Lan, R.; Irvine, J. T. S.; Tao, S., Synthesis of ammonia directly from air and water at ambient temperature and pressure. *Scientific Reports* **2013,** *3* (1), 1145.

166. Han, L.; Liu, X.; Chen, J.; Lin, R.; Liu, H.; Lü, F.; Bak, S.; Liang, Z.; Zhao, S.; Stavitski, E.; Luo, J.; Adzic, R. R.; Xin, H. L., Atomically Dispersed Molybdenum Catalysts for Efficient Ambient Nitrogen Fixation. *Angewandte Chemie International Edition* **2019,** *58* (8), 2321-2325.

167. Le, Y. Q.; Gu, J.; Tian, W. Q., Nitrogen-fixation catalyst based on graphene: every part counts. *Chem Commun (Camb)* **2014,** *50* (87), 13319-22.

168. Ling, C.; Bai, X.; Ouyang, Y.; Du, A.; Wang, J., Single Molybdenum Atom Anchored on N-Doped Carbon as a Promising Electrocatalyst for Nitrogen Reduction into Ammonia at Ambient Conditions. *The Journal of Physical Chemistry C* **2018,** *122* (29), 16842-16847.

169. Ling, C.; Niu, X.; Li, Q.; Du, A.; Wang, J., Metal-Free Single Atom Catalyst for N_2 Fixation Driven by Visible Light. *Journal of the American Chemical Society* **2018,** *140* (43), 14161-14168.

170. Mao, X.; Zhou, S.; Yan, C.; Zhu, Z.; Du, A., A single boron atom doped boron nitride edge as a metal-free catalyst for N_2 fixation. *Phys Chem Chem Phys* **2019,** *21* (3), 1110-1116.

171. Yu, X.; Han, P.; Wei, Z.; Huang, L.; Gu, Z.; Peng, S.; Ma, J.; Zheng, G., Boron-Doped Graphene for Electrocatalytic N_2 Reduction. *Joule* **2018,** *2* (8), 1610-1622.